

1 Temporary pause in the growth of atmospheric ethane and 2 propane in 2015-2018

3 **Hélène Angot^{1,2}, Connor Davel¹, Christine Wiedinmyer³, Gabrielle Pétron^{3,4}, Jashan**
4 **Chopra¹, Jacques Hueber^{1,5}, Brendan Blanchard¹, Ilann Bourgeois^{3,6}, Isaac Vimont³,**
5 **Stephen A. Montzka⁴, Ben R. Miller^{3,4}, James W. Elkins⁴, Detlev Helmig^{1,5}.**

6 ¹Institute of Arctic and Alpine Research, University of Colorado Boulder, Boulder, CO, USA.

7 ²Extreme Environments Research Laboratory, École Polytechnique Fédérale de Lausanne (EPFL) Valais Wallis, Sion,
8 Switzerland.

9 ³Cooperative Institute for Research in Environmental Sciences, University of Colorado Boulder, Boulder, CO, USA.

10 ⁴NOAA, Global Monitoring Laboratory (GML), Earth System Research Laboratories, Boulder, CO, USA.

11 ⁵Boulder A.I.R. LLC, Boulder, CO, USA.

12 ⁶NOAA, Chemical Sciences Laboratory (CSL), Earth System Research Laboratories, Boulder, CO, USA.

13 *Correspondence to:* Hélène Angot (helene.angot@epfl.ch)

14 **Abstract.**

15 Atmospheric non-methane hydrocarbons (NMHCs) play an important role in the formation of
16 secondary organic aerosols and ozone. After a multidecade global decline in atmospheric mole
17 fractions of ethane and propane – the most abundant atmospheric NMHCs – previous work has
18 shown a reversal of this trend with increasing atmospheric abundances from 2009 to 2015 in the
19 Northern Hemisphere. These concentration increases were attributed to the unprecedented growth
20 in oil and natural gas (O&NG) production in North America. Here, we supplement this trend
21 analysis building on the long-term (2008-2010; 2012-2020) high-resolution (~ 3-hour) record of
22 ambient air C₂-C₇ NMHCs from in-situ measurements at the Greenland Environmental
23 Observatory at Summit station (GEOSummit, 72.58°N, 38.48°W, 3210 m above sea level). We
24 confirm previous findings that the ethane mole fraction significantly increased by +69.0 [+47.4,
25 +73.2; 95 % confidence interval] ppt per year from January 2010 to December 2014. Subsequent
26 measurements, however, reveal a significant decrease by -58.4 [-64.1, -48.9] ppt per year from
27 January 2015 to December 2018. A similar reversal is found for propane. The upturn observed
28 after 2019 suggests, however, that the pause in the growth of atmospheric ethane and propane
29 might only have been temporary. Discrete samples collected at other northern-hemisphere baseline
30 sites under the umbrella of the NOAA cooperative global air sampling network show a similar

31 decrease in 2015-2018 and suggest a hemispheric pattern. Here, we further discuss the potential
32 contribution of biomass burning and O&NG emissions, the main sources of ethane and propane,
33 and we conclude that O&NG activities likely played a role in these recent changes. This study
34 highlights the crucial need for better constrained emission inventories.

35

36 **1. Introduction**

37 Non-methane hydrocarbons (NMHCs) are emitted to the atmosphere by a variety of biogenic and
38 anthropogenic sources. Their atmospheric oxidation contributes to the production of surface ozone
39 and aerosols, with impacts on air quality and climate forcing (Houweling et al., 1998). The
40 abundance of atmospheric NMHCs (ethane, propane, i-butane, n-butane, i-pentane, n-pentane)
41 increased steadily after 1950 until reduced emissions from oil and natural gas (O&NG) production
42 and emission regulations from diverse sources (*e.g.*, automobiles and industrial processes) were
43 implemented in the 1970s (Helmig et al., 2014). Emission reductions led to a gradual decline (3-
44 12 % per year) of NMHCs at urban and semi-rural sites in the last five decades (*e.g.*, von
45 Schneidemesser et al., 2010; Warneke et al., 2012). Accounting for an approximate atmospheric
46 lifetime (at $\text{OH} = 6.5 \times 10^5 \text{ molecules/cm}^3$) ranging from 4.5 days for pentanes to 2 months for
47 ethane, these emission reductions are also reflected in observations of background air composition,
48 as seen in Northern Hemisphere firn air records (Aydin et al., 2011; Worton et al., 2012; Helmig
49 et al., 2014): light alkanes increased steadily post 1950, peaking ~50 % above 1950 levels around
50 1970-1985, and then steadily declined until 2010 to levels that were close to 1950 levels. After
51 some 40 years of steadily declining atmospheric ethane and propane mixing ratios, Helmig et al.
52 (2016) reported a reversal in this behavior: the analysis of weekly discrete air samples showed that
53 between mid-2009 and mid-2014, ethane abundance at surface sites in the Northern Hemisphere
54 increased at a rate of 2.9-4.7 % per year. These observations and conclusions were further
55 substantiated by solar Fourier transform infrared (FTIR) ethane column retrievals showing similar
56 increases in the mid to upper tropospheric ethane column (Franco et al., 2015, 2016; Hausmann et
57 al., 2016). The largest increase rates for ethane and propane mixing ratios were found at sites
58 located in the Eastern United States (U.S.) and in the Northern Atlantic Region, indicating larger
59 emissions from the central to eastern parts of the U.S., with the likely sources being increased
60 emissions from shale O&NG extraction operations.

61 Interestingly, there is a strong latitudinal gradient of absolute NMHC dry air mole fractions – with
62 highest abundances in the Arctic where atmospheric removal rates are low during the polar winter
63 (Helmig et al., 2016, 2009; Rudolph, 1995). Despite the sensitivity of the Arctic to pollution
64 transport from lower latitudes, climate change, and already recognized and further anticipated
65 feedbacks on the global climate, long-term in-situ atmospheric composition observations within
66 the Arctic are sparse. A large part of our current knowledge of polar atmospheric chemistry stems
67 from research aircraft missions and campaign-type observations (e.g., Hartery et al., 2018; Jacob
68 et al., 2010; Law et al., 2014). However, long-term continuous measurements or regularly repeated
69 observations with consistent methodology and instrumentation are indispensable for establishing
70 a baseline record of environmental conditions at clean remote sites and for observing their changes
71 over time. Such data also serve as a legacy for future research that will rely on comparison with
72 archived observations of environmental conditions.

73 In that context, the National Oceanic and Atmospheric Administration (NOAA) Global
74 Monitoring Laboratory (GML) initiated a cooperative air-sampling network at Niwot Ridge,
75 Colorado, in 1967 (hereafter referred to as the NOAA/GML Carbon Cycle Greenhouse Gases
76 (CCGG) network (<https://www.esrl.noaa.gov/gmd/ccgg/>)). This network is nowadays an
77 international effort and discrete air samples are collected approximately weekly from a globally
78 distributed network of sites, including four Arctic sites: Utqiagvik (formerly known as Barrow,
79 Alaska, USA), Alert (Nunavut, Canada), Summit (Greenland), and Ny-Ålesund (Svalbard,
80 Norway). These samples are analyzed for CO₂, CH₄, CO, H₂, N₂O, and SF₆ at GML (e.g., Geller
81 et al., 1997; Komhyr et al., 1985; Steele, 1991), and at the University of Colorado Institute for
82 Arctic and Alpine Research (INSTAAR) for stable isotopes of CO₂ and CH₄ (Miller et al., 2002;
83 Trolier et al., 1996). These samples have also been analyzed for a variety of volatile organic
84 compounds (VOCs) including C₂-C₇ NMHCs at INSTAAR since 2004 (Pollmann et al., 2008;
85 Schultz et al., 2015). In 2014, measurements of ethane and propane were added to discrete air
86 samples collected under the umbrella of the NOAA/GML Halocarbons and other Atmospheric
87 Trace Species (HATS) network since 2004
88 (<https://www.esrl.noaa.gov/gmd/hats/flask/flasks.html>).

89 The discrete, typically weekly, air sampling by cooperative global networks have been at the
90 forefront of studies to identify and quantify long-term trends in the background air abundances of
91 important trace gases (e.g., Masarie and Tans, 1995; Montzka et al., 2018; Nisbet et al., 2014,

92 2019). In parallel, higher temporal-resolution in-situ measurements allow the investigation of
93 gases' variability and of shorter-term trends at specific sites. Here, we report in-situ 2 to 4-hourly
94 ambient air C₂-C₇ NMHCs dry air mole fractions from measurements at the Greenland
95 Environmental Observatory at Summit station (GEOSummit) by gas chromatography (GC) and
96 flame ionization detection (FID). Despite the advent of new methods based on optical
97 measurement (e.g., FTIR spectroscopy) and mass spectrometry (e.g., Photon-Transfer Mass
98 Spectrometry), GC-FID remains the dominant method in routine VOC observations due to its
99 stable long-term response characteristics and relatively low maintenance cost (Schultz et al., 2015).
100 NMHCs were first monitored with high temporal frequency at GEOSummit from 2008 to 2010
101 with support from the NASA Research Opportunities in Space and Earth Sciences (ROSES)
102 program (Kramer et al., 2015). NMHC monitoring resumed in 2012 as part of the National Science
103 Foundation (NSF) Arctic Observing Network program and was continuous and uninterrupted until
104 March 2020, providing one of the few high-temporal resolution long-term records of NMHCs in
105 the Arctic. In this paper, we investigate and discuss seasonal variations, rates of change, and
106 potential sources of NMHCs in the high Arctic. We also analyze multiyear trace gas data from
107 other background sites under the umbrella of the NOAA/GML CCGG and HATS sampling
108 networks to support our findings.

109

110 **2. Materials and Methods**

111 GEOSummit (72.58°N, 38.48°W, 3210 m above sea level) is a research facility located on the
112 Greenland ice sheet funded by the U.S. NSF and operated in collaboration with the Government
113 of Greenland (see Fig. 1). The station hosts a diverse array of Geoscience and Astrophysics
114 research projects (<https://www.geosummit.org/instruments>) and is the only high altitude remote
115 atmospheric observatory in the Arctic. Ambient air is monitored at the Temporary Atmospheric
116 Watch Observatory (TAWO) located ~ 1 km south of the research camp.

117 **2.1 In-situ NMHC measurements**

118 C₂-C₇ NMHCs (ethane, propane, iso-butane, n-butane, acetylene, iso-pentane, n-pentane, n-
119 hexane, benzene, toluene) were analyzed from July 2008 to July 2010 and from May 2012 to
120 March 2020 by GC-FID using a fully automated and remotely controlled custom-built system.
121 Ambient air was continuously sampled from a 10 m high inlet on the meteorological tower adjacent
122 to the TAWO building through a heated (~30°C) sampling line. The sampling frequency increased

123 from 6 ambient NMHC runs to 12 daily runs in 2018. The GC-FID system, tailored towards the
124 remote, unattended and long-term operation, is a further development of the instrument described
125 in detail by Tanner et al. (2006) and Kramer et al. (2015). The instrument relies on a cryogen-free
126 sample enrichment and injection system. Air was pulled from the tower inlet, and aliquots of the
127 sample stream were first passed through a water trap (u-shaped stainless-steel treated Silcosteel™
128 tube cooled using thermoelectric coolers) to dry the sample to a dew point of -20°C, and NMHCs
129 were then concentrated on a Peltier-cooled (-35°C) multi-stage adsorbent trap. Analysis was
130 accomplished by thermal desorption and injection onto an Al₂O₃ PLOT column for cryogen-free
131 separation on an SRI Model 8610 GC-FID. Our monitoring effort followed the World
132 Meteorological Organization (WMO) Global Atmospheric Watch (GAW) quality control
133 guidelines: blanks and calibration standards were injected every other day from the manifold and
134 processed in the exact same way as ambient samples. The limit of detection was ~2 ppt (pmol/mol
135 by volume) for all compounds and no significant blank contamination was ever noticed.
136 Quantification was based on monthly FID response factors (Scanlon and Willis, 1985) calculated
137 from the repeated analysis of two independently prepared and cross-referenced standards in use at
138 any given time. Tables S1 and S2 summarize these response factors along with the associated
139 relative standard deviation (< 5 % on average for all compounds) for 2008-2010 and 2012-2020,
140 respectively. The in-situ GC-FID system provided a stable response from 2008 to 2020, with
141 monthly response factors varying by ≤ 5 % for ethane, propane, and butanes, and by ≤ 20 % for
142 other compounds over this period. The monitoring program was audited by the World Calibration
143 Center for Volatile Organic Compounds at the site in July 2017 ([https://www.imk-ifu.kit.edu/wcc-](https://www.imk-ifu.kit.edu/wcc-voc/)
144 [voc/](https://www.imk-ifu.kit.edu/wcc-voc/)). All reported VOCs results were found to be within the Global Atmospheric Watch program
145 quality objectives (WMO, 2007).

146 **2.2 Discrete measurements**

147 We used NMHC data from Alert, Utqiagvik, Mace Head (Ireland), Park Falls (Wisconsin, USA),
148 and Cape Kumukahi (Hawaii, USA; see Fig. 1) collected as part of the NOAA/GML CCGG
149 (October 2004 to August 2016) and HATS (August 2014 to March 2020) sampling and
150 measurement programs. Note that we combined here measurements from the two networks.

151 **2.2.1 CCGG discrete sampling and analysis**

152 As described by Steele et al. (1987) and Dlugokencky et al. (1994), air samples are collected
153 ~weekly in pairs in 2.5 L borosilicate flasks with two glass-piston stopcocks sealed with Teflon

154 O-rings. Flasks are flushed in series for 5 to 10 minutes and then pressurized to ~1.2 atm with a
155 portable sampling system. Samples collected from October 2004 to August 2016 were analyzed at
156 INSTAAR in Boulder, Colorado, by GC-FID. The analysis, on a HP-5890 series II gas
157 chromatograph, first involved drying of approximately 600 cubic centimeter (cc) of sample gas by
158 running the sample gas through a 6.4 mm (outer diameter) stainless steel tube cooled to -25°C.
159 The analytes were then preconcentrated at -35°C on an adsorbent bed (Carboxen 1000/1016).
160 Samples were thermally desorbed at 310°C onto a short capillary guard column before separation
161 on an Al₂O₃ PLOT capillary column (0.53 mm × 60 m). Weekly instrument calibrations were
162 performed using primary calibration standards acquired from the NOAA Global Monitoring
163 Laboratory, the U.K. National Physics Laboratory, and the U.S. National Institute of Technology.
164 These standards scales have been maintained since 2006 by regular inter-comparison and
165 propagation of the scale with newly acquired standards. Deviations in the response factors from
166 these different standards were smaller than 5 %, with results for ethane and propane typically being
167 equal or having less than 2-3 % deviation. Instrument FID response is linear within the range of
168 observed ambient concentrations. The INSTAAR NMHC laboratory was audited by the WMO
169 GAW World Calibration Center for VOCs (WCC-VOC, <https://www.imk-ifu.kit.edu/wcc-voc/>) in
170 2008 and in 2016, and both times all measurement results passed the WMO data quality criteria
171 (WMO, 2007).

172 2.2.2 HATS discrete sampling and analysis

173 At GEOSummit, paired borosilicate glass flasks are also pressurized to ~1 atmosphere
174 overpressure with ambient air as part of the HATS sampling program. At other NH sites,
175 electropolished stainless-steel flasks are used. All flasks are analyzed by GC with mass
176 spectrometry analysis with a preconcentration system similar to Miller et al. (2008) to strip water
177 vapor and CO₂ from the airstream prior to injection of condensates (VOCs, halocarbons, solvents,
178 and other gases) onto a 0.32 mm (inner diameter) GasPro capillary column. Results are tied to a
179 suite of standards prepared in-house with gravimetric techniques.

180 **2.3 Ancillary data**

181 Continuous monitoring of carbon monoxide (CO) was conducted at GEOSummit between May
182 2019 and March 2021 with a cavity ring-down spectroscopy (CRDS) analyzer (Picarro G-2401).
183 A switching manifold allowed regular sampling of ambient air and calibration gases. Three NOAA
184 GML standards were integrated into the automated calibration. Low (69.6 ppb) and high (174.6

185 ppb) calibration points were performed for ~3 minutes every two days, while an intermediate
186 (117.4 ppb) calibration was carried out in between. Using the last minute of each calibration, the
187 low and high calibration points were used to determine the linear relationship between the certified
188 calibration values and the analyzer's reported calibration values. The calibration offset (slope and
189 intercept) was calculated and used to correct the third intermediate calibration point. The mean
190 absolute difference between the corrected and certified intermediate calibration paired values was
191 1.6 ppb, *i.e.*, 1.4 %. The minute-averaged CRDS CO ambient air data were corrected using the
192 calibration offset. The CRDS has a manufacturer-specified precision at 5 seconds, 5 minutes, and
193 60 minutes of 15, 1.5, and 1 ppb for CO (G2401 Gas Concentration Analyzer | Picarro, 2020).
194 We also use ethane, propane, tetrachloroethylene (C₂Cl₄), and hydrogen cyanide (HCN) data
195 collected in the free troposphere during the global-scale airborne Atmospheric Tomography
196 mission (ATom; <https://espo.nasa.gov/atom/content/ATom>) onboard the NASA DC-8 aircraft
197 (Wofsy et al., 2018). Canisters collected with the University of California Irvine Whole Air
198 Sampler (WAS) were analyzed for more than 50 trace gases, including ethane, propane, and
199 tetrachloroethylene by GC-FID and GC-mass spectrometric detection (Barletta et al., 2020).
200 Hydrogen cyanide was measured in situ with the California Institute of Technology Chemical
201 Ionization Mass Spectrometer (CIT-CIMS; Allen et al., 2019). For the purpose of our analysis, we
202 removed data collected over continents, in the marine boundary layer (altitude < 0.4 km), or
203 corresponding to stratospheric air (ozone to water vapor ratio > 1 ppb per ppm).

204 **2.4 Curve fitting method and trend analysis**

205 We used the curve fitting method developed by Thoning et al. (1989) and described in detail at
206 <https://www.esrl.noaa.gov/gmd/ccgg/mbl/crvfit/crvfit.html>. Briefly, the data were fitted with a
207 function consisting of a polynomial and series of harmonics to represent the average long-term
208 trend and seasonal cycle. Residuals from the function were calculated, transformed into frequency
209 domain with a fast Fourier transform algorithm, then filtered with two low pass filters. One
210 eliminates harmonics less than ~1 month. When converted back to time domain and added to the
211 function, it gives a smoothed curve. The other filter eliminates periods less than ~1 year; when
212 transformed back to time domain and added to the polynomial, it gives the deseasonalized trend
213 (hereafter referred to as the trend). The Sen's slope estimate of the trend was calculated using
214 function TheilSen in R package openair (Carslaw and Ropkins, 2012). Note that the p-values and

215 all uncertainties are calculated through bootstrap simulations
216 (<https://davidcarslaw.github.io/openair/reference/TheilSen.html>).

217 **2.5 Source apportionment analysis**

218 In order to identify potential source regions, we performed a Potential Source Contribution
219 Function (PSCF) analysis using the *trajLevel* function in R package openair (Carslaw and Ropkins,
220 2012). Based on air-mass back-trajectories (see below) and NMHC residuals (see Section 2.4), the
221 PSCF calculates the probability that a source is located at latitude i and longitude j . PSCF solves:

$$222 \quad PSCF = m_{ij}/n_{ij} \quad \text{Eq.1}$$

223 where n_{ij} is the number of times that the trajectories passed through the cell (i, j) and m_{ij} the
224 number of trajectories passing through that cell in which the NMHC residual was greater than a
225 given threshold (90th percentile of the measured results distribution). Note that cells with very few
226 trajectories passing through them have a weighting factor applied to reduce their effect.

227 For each NMHC in-situ measurement, HYSPLIT (HYbrid Single Particle Lagrangian Integrated
228 Trajectory; Draxler and Rolph, 2013) 5-day air-mass back trajectories used in the PSCF analysis
229 were generated using the Python package *pysplit* (Warner, 2018) and processor *pysplitprocessor*
230 available at: <https://github.com/brendano257/pysplit> and
231 <https://github.com/brendano257/pysplitprocessor>, respectively. The HYSPLIT Lagrangian
232 particle dispersion model was run from April 2012 to June 2019 using the National Center for
233 Environmental Prediction Global Data Assimilation System (NCEP GDAS) $0.5^\circ \times 0.5^\circ$
234 meteorological inputs available at: <ftp://arlftp.arlhq.noaa.gov/pub/archives/gdas0p5>. We did not
235 generate back-trajectories for observations after June 2019 due to the unavailability of the GDAS
236 $0.5^\circ \times 0.5^\circ$ archive.

237

238 **3. Results and Discussion**

239 **3.1 Seasonal variation**

240 The seasonal variation of C₂-C₇ NMHCs at GEOSummit is displayed in Fig. 2. Summer refers to
241 June-August, fall to September-November, winter to December-February, and spring to March-
242 May. NMHCs exhibit a strong and consistent seasonal pattern year after year, with maximum mole
243 fractions during winter and early spring, and a rapid decline towards summer. Anthropogenic
244 sources of NMHCs do not vary much seasonally (Pozzer et al., 2010). Therefore, the observed
245 seasonal cycle is primarily driven by the seasonally changing sink strength by reaction with the

246 photochemically formed OH radical (Goldstein et al., 1995) – the dominant oxidizing agent in the
247 global troposphere (Levy, 1971; Logan et al., 1981; Thompson, 1992). During the summer period,
248 mole fractions of the heavier NMHCs were below or close to the detection limit (Fig. 2b). As
249 already noted by Goldstein et al. (1995) and Kramer et al. (2015) based on a limited dataset, the
250 phase of each NMHC is shifted due to the rate of reaction with OH. Ethane, the lightest and longest
251 lived of the NMHCs shown in Fig. 2, peaks in February/March with a median of 2110 ppt, and
252 declines to a minimum of 734 ppt in July. Heavier and shorter-lived NMHCs have lower mole
253 fractions, peak earlier in the year (January/February), and reach a minimum earlier in summer
254 (June) due to their faster rate of reaction with OH (Chameides and Cicerone, 1978).
255 Because changes in NMHC sources and sinks can affect the seasonal cycle amplitude, we
256 investigated whether there is a trend in the NMHC's amplitude at GEOSummit. We focus here on
257 ethane and propane, the most abundant hydrocarbons in the remote atmosphere after methane.
258 Figure 3 shows the amplitude of the ethane and propane seasonal cycles, determined as the relative
259 difference between the maximum and minimum values from the smooth curve for each annual
260 cycle (Dlugokencky et al., 1997). The peak-to-minimum relative amplitude ranged from 64 to 71
261 % for ethane and from 92 to 96 % for propane, and there is no indication of a significant overall
262 trend in amplitude. This range of amplitudes is in good agreement with the literature: the typical
263 seasonal amplitudes for ethane are on the order of 50 % at mid-latitude sites and can increase up
264 to 80 % at remote sites (Franco et al., 2016; Helmig et al., 2016). Changes in mole fractions are
265 further investigated and discussed in the following section.

266 **3.2 Reversal of ethane and propane rates of change at GEOSummit in 2015**

267 Ethane is released from seepage of fossil carbon deposits, volcanoes, fires, and from human
268 activities – with O&NG extraction, processing, distribution, and industrial use being the primary
269 sources (Pozzer et al., 2010). Based on the inventory developed for the Hemispheric Transport of
270 Air Pollutants, Phase II (HTAP2, Janssens-Maenhout et al., 2015), biogenic emissions from
271 MEGAN2.1 (Guenther et al., 2012), and fire emissions from FINNv1.5 (Wiedinmyer et al., 2011),
272 Helmig et al. (2016) estimated that ~4 %, 18 %, and 78 % of global ethane emissions are due to
273 biogenic, biomass burning, and anthropogenic sources, respectively. Global ethane emission rates
274 decreased by 21 % from 1984 to 2010 likely due to decreased venting and flaring of natural gas in
275 oil producing fields (Simpson et al., 2012). As a consequence, atmospheric ethane background air
276 mixing ratios significantly declined during 1984-2010, by an average of -12.4 ± 1.3 ppt per year

277 in the Northern Hemisphere (Aydin et al., 2011; Worton et al., 2012; Helmig et al., 2014).
278 However, the analysis by Helmig et al. (2016) of ten years (2004-2014) of NMHC data from air
279 samples collected at NOAA GML remote global sampling sites (including GEOSummit) showed
280 a reversal of the global ethane trend from mid-2009 to mid-2014 (ethane growth rates > 50 ppt per
281 year at 32 sites). This trend reversal was attributed to increased U.S. O&NG production (Helmig
282 et al., 2016). Figure 4a shows the July 2008-March 2020 ethane trend at GEOSummit, as inferred
283 from our in-situ measurements (dotted line). Note that the same time-series but also showing
284 individual data points can be found in Fig. S1. Ethane mixing ratios at GEOSummit significantly
285 (p-value < 0.001) increased by +69.0 [+47.4, +73.2; 95 % confidence interval] ppt per year from
286 January 2010 to December 2014. A reversal is, however, evident after 2015: ethane mixing ratios
287 significantly (p-value < 0.001) decreased by -58.4 [-64.1, -48.9] ppt per year from January 2015
288 to December 2018. Data collected after 2019, however, suggest that the pause in the growth of
289 atmospheric ethane might only be temporary. We focus hereafter on the 2015-2018 reversal period.
290 Similar to ethane, a reversal is evident late 2014 for propane (see Fig. 4b; dotted line): mixing
291 ratios significantly (p-value < 0.001) increased by +47.9 [+32.3, +52.3] ppt per year from January
292 2010 to June 2014, but significantly (p-value < 0.001) decreased at a rate of -70.5 [-76.1, -65.8]
293 ppt per year from July 2014 to July 2016. Propane mixing ratios remained fairly stable (+10.2
294 [+6.6, +14.6] ppt per year; p-value < 0.001) from July 2016 to December 2019. It should be noted
295 that the pause in the growth of atmospheric ethane and propane at GEOSummit in 2015-2018 is
296 confirmed by independent discrete sampling under the umbrella of the NOAA/GML CCGG and
297 HATS networks (see Fig. 4; solid lines). Figure S2 shows the good agreement ($R^2 = 0.97$ for
298 ethane, $R^2 = 0.99$ for propane) between in-situ GC-FID measurements and discrete samples.
299 The temporary pause in the growth of ethane and propane at GEOSummit could either suggest
300 changes in: i) the OH sink strength, ii) atmospheric transport from source regions and/or iii)
301 natural/anthropogenic emissions.
302 The tropospheric abundance of OH is driven by a complex series of chemical reactions involving
303 tropospheric ozone, methane, carbon monoxide, NMHCs, and nitrogen oxides, and by the levels
304 of solar radiation and humidity (Logan et al., 1981; Thompson, 1992). Building on the comparison
305 of modeled and observed methane and methyl chloroform lifetimes, Naik et al. (2013) showed that
306 OH concentrations changed little from 1850 to 2000. The authors suggested that the increases in
307 factors that enhance OH (humidity, tropospheric ozone, nitrogen oxide emissions, and UV

308 radiation) was compensated by increases in OH sinks (methane abundance, carbon monoxide and
309 NMHC emissions). More recently, Naus et al. (2020) used a 3D-model inversion of methyl
310 chloroform to constrain the atmospheric oxidative capacity – largely determined by variations in
311 OH – for the period 1998-2018. The authors showed that the interannual variations were typically
312 small (<3 % per year) and found no evidence of a significant long-term trend in OH over the study
313 period. Changes in NMHC mole fractions at GEOSummit are well outside what could be explained
314 by a 3% change in OH tropospheric concentrations. There is, however, likely a difference between
315 global and regional OH variations (Brenninkmeijer et al., 1992; Spivakovsky et al., 2000;
316 Lelieveld et al., 2004). In the absence of data on the Arctic and mid-latitudes OH abundance, we
317 concede that OH may play a role on the observed pause but do not discuss that hypothesis further.
318 The latter two hypotheses are investigated and verified or rejected in the following sections.

319 **3.3 Changes in transport from source regions**

320 The synoptic-scale tropospheric circulation in the Arctic is driven by three major semi-permanent
321 pressure systems: i) the Aleutian Low, low-pressure center located south of the Bering Sea area,
322 ii) the Icelandic Low, low-pressure system located southeast of Greenland near Iceland, and iii)
323 the Siberian High, high-pressure center located over eastern Siberia (Barrie et al., 1992). During
324 positive phases of the North Atlantic Oscillation (NAO), the Icelandic Low is strengthened and
325 transport into the Arctic enhanced, resulting in higher Arctic pollution levels (Duncan and Bey,
326 2004; Eckhardt et al., 2003). Negative phases of the NAO are associated with decreased transport
327 from Europe and Siberia and an increased relative contribution from North America (Octaviani et
328 al., 2015). In addition, mid-latitude atmospheric blocking events – quasi-stationary features
329 characterized by a high-pressure cell centered around 60°N and lasting up to ~15 days (Rex, 1950)
330 – are known to enhance transport of polluted air to the Arctic (Iversen and Joranger, 1985). Here,
331 we test the hypothesis of a pause in the growth of atmospheric ethane and propane at GEOSummit
332 driven by the interannual variability of pollution transport from source regions. We investigated
333 the potential influence of the NAO using monthly mean values from the NOAA Climate Prediction
334 Center. We found a somewhat weak but significant positive correlation between the NAO and
335 monthly-averaged mixing ratios over the 2008-2019 period ($R^2 = 0.4$, p-value < 0.01 for both
336 ethane and propane), in line with enhanced transport of pollution to the Arctic during positive
337 phases of the NAO. We also investigated the potential influence of the Northern Annular Mode
338 (NAM), which has a strong interannual component (Hu and Feng, 2010). We found a low

339 correlation between the NAM and monthly-averaged mixing ratios ($R^2 < 0.2$, p-value = 0.1 for
340 both ethane and propane). Previous studies have shown that the influence of the NAM varies by
341 regional section of the Arctic; while persistent organic pollutants concentrations were found to
342 correlate with NAM phases at Ny-Ålesund (Svalbard), no correlation was found at Alert (Nunavut,
343 Canada) (Becker et al., 2008; Octaviani et al., 2015).

344 Figure 5 shows the origin of air masses influencing GEOSummit (annual gridded back trajectory
345 frequencies) and Figure 6a summarizes the relative contribution of each geographical sector for
346 each year. Contrary to other Arctic sites (Hirdman et al., 2010), GEOSummit is mostly influenced
347 by transport from North America and Europe, whereas Siberia has relatively little influence (0-2
348 %). These results are in agreement with the isobaric 10-day back-trajectory study by Kahl et al.
349 (1997) and the 20-day backward FLEXPART simulations by Hirdman et al. (2010). European air
350 masses represented 3-6 % of the total, with a 10 % high in 2018. The relative contribution of North
351 Atlantic air masses (“ocean”) ranged from 1 to 9 %, with a 14 % high from January to August
352 2019. The frequency of North American air masses exhibited the most variability, ranging from 2
353 to 20 %. Years with enhanced transport from North America (e.g., 2012, 2019) coincided with a
354 negative NAO index, known to drive decreased (increased) relative contribution from Europe/Asia
355 (North America) (Octaviani et al., 2015). Assuming that the ethane and propane trends are driven
356 by emissions in North America (Helmig et al., 2016) and that these emissions are constant, one
357 would expect higher ethane and propane mixing ratios in years when the relative influence of
358 North American air masses peaked. There is, however, an anticorrelation: a 2-3 % relative
359 contribution of North American air masses in 2014 and 2015 when ethane/propane mixing ratios
360 reached a maximum, and 19 % in 2018 when mixing ratios reached a minimum. This leaves two
361 possibilities: either North American emissions dropped over the studied time period (see Section
362 3.4), or ethane/propane trends observed at GEOSummit are not driven by emissions in North
363 America (see below).

364 The relative contribution of local/regional air masses (*i.e.*, around Greenland, see Fig. 5) increased
365 from 79 % in 2012 to 91-93 % in 2014-2015 before gradually dropping to 61 % in 2018. The
366 apparent correlation between the relative contribution of local/regional air masses and the
367 ethane/propane trend raises the question of whether these are connected. In order to identify
368 potential sources in this sector, we performed a PSCF analysis to investigate source-receptor
369 relationships (e.g., Pekney et al., 2006; Perrone et al., 2018; Yu et al., 2015; Zhou et al., 2018;

370 Zong et al., 2018). The PSCF calculates the probability that a source is located at latitude i and
371 longitude j (Pekney et al., 2006). Figure S3 shows the results of the PSCF analysis for ethane and
372 propane residuals and shows no consistent pattern associated with elevated concentrations. In both
373 winter and summer, the probability of an ethane or propane source from this analysis is low (<2
374 % on average).

375 The history of petroleum exploration activities on the Greenland continental shelf dates back to
376 the 1970s (Arctic Oil & Gas Development: The Case of Greenland, 2020). More recently, the
377 Greenland's government announced the opening of three new offshore areas for exploration in
378 November 2020 (Greenland Opens Offshore Areas for Drilling, 2020). Despite exploration drilling
379 activities, there has never been any O&NG exploitation of Greenland resources (Arctic Oil &
380 Gas Development: The Case of Greenland, 2020). Building on the above, the possibility of a
381 significant local/regional source can be ruled out, and so can the hypothesis that the pause in the
382 growth of ethane and propane is driven by local/regional emissions. The last remaining hypothesis
383 is that this pause is due to a change in emissions from any of the other source sectors, or a
384 combination of them, or total NH emissions and associated change in baseline NH atmospheric
385 levels. This hypothesis is tested in the following Section using observations at other baseline sites.

386 **3.4 Evidence for a hemispheric pattern**

387 Table 1 summarizes the rate of change and 95 % confidence interval for 2010-2014 and 2015-
388 2018 at Alert (ALT, Nunavut, Canada), Utqiagvik/Barrow (BRW, Alaska, USA), Cape Kumukahi
389 (KUM, Hawaii, USA), Park Falls (LEF, Wisconsin, USA), and Mace Head (MHD, Ireland – see
390 Fig. 1) where discrete samples were collected for the NOAA/GML CCGG and HATS cooperative
391 networks. The ethane and propane time-series at the various sites are shown in Figures S4 and S5,
392 respectively. A clear reversal in interannual changes for ethane and propane mixing ratios is
393 observed in 2015 at ALT, BRW, KUM, and LEF. These results support the observed changes at
394 GEOSummit and indicate a hemispheric pattern, likely due to a change in Northern Hemisphere
395 emissions, with a turning point around late 2014. Biomass burning and anthropogenic activities
396 being the main emitters of NMHCs, we hereafter focus the discussion on these two sources.

397 **3.4.1 Biomass burning**

398 Occasional biomass burning plumes were observed at GEOSummit. For example, Fig. 7 shows
399 the simultaneous increase in CO, ethane, propane, and benzene mixing ratios for a short number
400 of days in July and August 2019. According to the Whole Atmosphere Community Climate Model

401 (WACCM; Gettelman et al., 2019) CO forecast simulations, available at
402 <https://www.acom.ucar.edu/waccm/forecast/>, these enhancements can be attributed to intense
403 Siberian wildfires occurring at that time (Bondur et al., 2020). In good agreement with the
404 WACCM simulations, emission ratios (amount of compound emitted divided by that of a reference
405 compound) derived from these two plumes for ethane and propane ($5.4\text{-}5.9 \times 10^{-3}$ and $1.5\text{-}1.6$
406 $\times 10^{-3}$ ppb per ppb of CO, respectively; see Fig. S6) are within the range of values reported for
407 boreal forest and peat fires (Andreae, 2019).

408 Despite the observation of occasional plumes at GEOSummit, the question remains whether
409 biomass burning could drive the observed hemispheric pause in the growth of atmospheric ethane
410 and propane. For ethane, the sensitivity to biomass burning emissions from boreal fires is almost
411 entirely balanced by the larger magnitude of emissions from non-boreal fires (Nicewonger et al.,
412 2020). For propane, being shorter-lived, the fire component over Greenland should be dominated
413 by emissions from boreal fires. We thus investigated the interannual variability of biomass burning
414 emissions from both all open burning north of 45°N (boreal fires) and north of the equator (all NH
415 fires). Figure 6b gives annual biomass burning emissions according to the Fire INventory from
416 NCAR (FINNv2.2) emission estimates driven by MODIS fire detections (Wiedinmyer et al., in
417 prep). Emissions north of 45°N peaked in 2012, known for being an exceptional wildfire season
418 in North America (e.g., Lassman et al., 2017; Val Martin et al., 2013). NH ethane and propane
419 emissions slightly decreased in 2017 and 2018 but were fairly stable over the 2008-2016 time
420 period. We did not find any significant correlation between annual biomass burning emissions and
421 annually-averaged mixing ratios (using either 2009-2018 or 2015-2018 data, and using either all
422 open burning north of 45°N or north of the equator). The seasonal analysis of the correlation
423 between ambient air mixing ratios and biomass burning emissions yielded similar results. This
424 suggests that the observed pause in the growth of atmospheric ethane and propane is likely not
425 driven by biomass burning emissions.

426 This conclusion is further supported by measurements during the aircraft mission ATom over the
427 Pacific and Atlantic Oceans. Using ethane and propane data collected in the Northern Hemisphere
428 ($>20^{\circ}\text{N}$) remote free troposphere during the four ATom seasonal deployments (July-August 2016,
429 January-February 2017, September-October 2018, and April-May 2018), we found a significant
430 positive correlation of ethane and propane with tetrachloroethylene ($R^2 = 0.6$, $p\text{-value} < 0.001$) and
431 a poor correlation with hydrogen cyanide ($R^2 < 0.1$, $p\text{-value} < 0.001$; see Fig. S7), used as tracers

432 of anthropogenic and biomass burning emissions, respectively (Bourgeois et al., in review). These
433 results from the remote free troposphere confirm that atmospheric ethane and propane ambient air
434 levels are mostly driven by anthropogenic activities rather than by biomass burning emissions, in
435 line with results from other studies (e.g., Xiao et al., 2008).

436 3.4.2 O&NG activities

437 Discrete samples collected at northern-hemisphere baseline sites show that the strongest change
438 was observed at LEF, located downwind from the Bakken oil field in North Dakota (Gvakharia et
439 al., 2017), with an increase of ethane mixing ratios of +167.7 [+157.5, +186.0] ppt per year in
440 2010-2014 and a decrease of -247.8 [-312.2, -158.2] ppt per year in 2015-2018 (see Table 1). This
441 result, along with previous findings by Helmig et al. (2016) and Franco et al. (2015), supports the
442 hypothesis that U.S. O&NG emissions could play a major role in driving atmospheric ethane and
443 propane concentrations in the NH. Here we further discuss this potential contribution to the
444 observed hemispheric pause in the growth of atmospheric ethane and propane in 2015-2018.

445 The U.S. has experienced dramatic increases in O&NG production since 2005, underpinned by
446 technological developments such as horizontal drilling and hydraulic fracturing (Caporin and
447 Fontini, 2017; Feng et al., 2019). This shale revolution has transformed the U.S. into the world's
448 top O&NG producer (Gong, 2020). Coincident with the shale gas boom, the U.S. production of
449 natural gas liquids (ethane, propane, butane, iso-butane, and pentane) has significantly increased
450 in the past decade from 0.6-0.7 billion barrels in the 2000s to 1.1 billion barrels in 2014, and close
451 to 1.8 billion barrels in 2019 (U.S. Field Production of Natural Gas Liquids, 2021). The main
452 source of ethane and propane has been identified to be leakage during the production, processing,
453 and transportation of natural gas (Tzompa-Sosa et al., 2019; Pétron et al., 2012; Roest and Schade,
454 2017).

455 Propane is extracted from natural gas stream and used as a heating fuel. As shown in Figure 8, the
456 U.S. propane field production temporarily plateaued from June 2014 to December 2016 (U.S. Field
457 Production of Propane, 2021) due to a slowdown in natural gas production in response to low
458 natural gas prices. As we consider recent changes in emissions, however, changes in emissions per
459 unit of production must also be considered. A recent study in the Northeastern Colorado Denver-
460 Julesburg Basin showed little change in atmospheric hydrocarbons, including propane, in 2008-
461 2016 despite a 7-fold increase in oil production and nearly tripling of natural gas production,
462 suggesting a significant decrease in leak and/or venting rate per unit of production (Oltmans et al.,

463 2021). While we cannot reliably estimate how propane emissions might have changed during this
464 recent period, these two influences, combined together, could explain the observed temporary
465 pause in the growth of atmospheric propane.

466 Estimating the total production, and ultimately emissions of ethane, is even more complex as it
467 depends on the ethane-to-natural gas price differential. Ethane has long been considered an
468 unwanted byproduct of O&NG drilling, much of it burned away in the natural gas stream or flared
469 off at well sites. Today, ethane is a key feedstock for petrochemical manufacturing and the U.S. is
470 currently the world's top producer and exporter of ethane (Sicotte, 2020). Depending on the price
471 of ethane relative to natural gas, ethane can be left in the natural gas stream and sold along with
472 natural gas – a process known as ethane rejection, or separated at natural gas processing plants
473 along with other natural gas liquids (such as propane). Assuming the same leak rates for ethane as
474 for methane, 85 % of ethane emissions are due to natural gas extraction and processing, while
475 processed natural gas transportation and use only represent 15 % of the natural gas supply chain
476 ethane loss rate (Alvarez et al., 2018). The slowdown in natural gas production from June 2014 to
477 December 2016 (see above) may thus have contributed to the atmospheric ethane plateauing.
478 However, these estimates do not take into account emissions of ethane from its own supply chain
479 (e.g., separation, storage, liquefaction for export, ethane cracker to produce ethylene and plastic
480 resins) – for which leak rates remain unknown. A number of top-down studies, focusing on specific
481 regions or time-periods (e.g., 2010-2014), have shown that current inventories underestimate
482 ethane emissions (e.g., Tzompa-Sosa et al., 2017; Pétron et al., 2014). The modeling study led by
483 Dalsøren et al. (2018) focusing on year 2011 claimed that fossil fuel emissions of ethane are likely
484 biased-low by a factor of 2-3. In this highly dynamic context, where ethane production and volume
485 rejected continuously vary and where leak rates change over time (Schwietzke et al., 2014), there
486 is a need for further hemispheric- or global-scale top-down studies focusing on the interannual
487 variability of ethane emissions.

488

489 **4. Summary and Conclusion**

490 Ethane and propane are the most abundant atmospheric NMHCs and they exert a strong influence
491 on tropospheric ozone, a major air pollutant and greenhouse gas. Increasing levels have been
492 reported in the literature from 2009 to 2014, with evidence pointing at U.S. O&NG activities as
493 the most likely cause (Kort et al., 2016; Helmig et al., 2016; Franco et al., 2016; Hausmann et al.,

494 2016). The long-term high-resolution records of ambient air C₂-C₇ NMHCs at GEOSummit
495 presented here confirm that atmospheric ethane and propane levels increased in the remote arctic
496 troposphere from 2009 to 2015, but also reveal a pause in their growth in 2015-2018. Using
497 independent discrete samples collected at other NH baseline sites, we show that this pause is
498 observed throughout the northern hemisphere – suggesting a change in total NH emissions and in
499 baseline NH atmospheric levels. We further investigated and discussed the contribution of the two
500 main NMHC emitters: biomass burning and O&NG production. We did not find any correlation
501 between atmospheric ethane and propane mixing ratios and the FINNv2.2 biomass burning
502 emission estimates. Additionally, data collected in the NH remote free troposphere during the
503 ATom aircraft campaign support that atmospheric ethane and propane ambient air levels are
504 mostly driven by anthropogenic activities rather than by biomass burning emissions. The fact that
505 the strongest rate of change reversal was observed at a site located downwind from the Bakken oil
506 field in North Dakota tends to suggest that U.S. O&NG activities yet again played a major role
507 here. The slowdown in U.S. natural gas production from June 2014 to December 2016 combined
508 with a decrease in leak rate per unit of production could have contributed to the observed temporary
509 pause. This conclusion is, however, tentative given the large uncertainties associated with emission
510 estimates, especially with ethane emissions from its supply chain. We hope this work can be used
511 as a starting point to understand what led to the pause in the growth of atmospheric ethane and
512 propane in 2015-2018 and, more generally, to what extent ON&G activities could be responsible
513 for variations in NH baseline ethane and propane levels.

514

515 **Data availability**

516 All non-methane hydrocarbons and carbon monoxide in-situ data used in this study are archived
517 and publicly available on the Arctic Data Center database (Angot et al., 2020; Helmig, 2017).
518 NOAA/GML HATS and CCGG discrete data are available at
519 <ftp://aftp.cmdl.noaa.gov/data/hats/PERSEUS> and ftp://aftp.cmdl.noaa.gov/data/trace_gases/voc/,
520 respectively.

521

522 **Author contribution**

523 DH initiated the long-term monitoring effort at GEOSummit and secured funding over the years.
524 JH designed and built the GC-FID used for NMHC in-situ monitoring and performed ~bi-annual

525 on-site visits for maintenance and calibration operations. CD, JC, and BB performed the in-situ
526 data processing (*i.e.*, GC peak identification, peak integration, background subtraction, and
527 calculation of mixing ratios). CD, JC, and HA analyzed the data under the supervision of CW and
528 DH. GP helped evaluating the impact ON&G activities on NMHC trends while IB and CW helped
529 evaluating the impact of biomass burning. IV, SAM, BRM and JWE provided the NOAA /GML
530 HATS discrete data. JH and DH provided the NOAA/GML CCGG NMHC discrete data with
531 contribution from CD, JC, and BB. HA wrote the manuscript with contribution from all co-authors.

532

533 **Competing interests**

534 The authors declare no competing interests.

535

536 **Acknowledgements**

537 We would like to thank the GEOSummit Science Technicians and CH2MHill Polar Services for
538 their tremendous support in enabling on-site and flask collections at the station. HA, JH, and DH
539 would like to acknowledge Maria Soledad Pazos, Miguel Orta Sanchez, and all students involved
540 in the NMHC flask analysis at INSTAAR. IV, SAM, and BRM thank the instrumental analysis
541 assistance of C. Siso and M. Crotwell and standards prepared and maintained by B. Hall at the
542 NOAA GML. We would also like to thank Donald Blake, Paul Wennberg, Michelle Kim, Hannah
543 Allen, John Crouse, and Alex Teng for the ATom dataset used in this analysis.

544

545 **Financial support**

546 The long-term observations and analysis efforts were supported by the US National Science
547 Foundation (grant nos. 1108391 and 1822406) and the NASA ROSES program (grant no.
548 NNX07AR26G). HA also received financial support from the Swiss National Science Foundation
549 (grant no 200021_188478). Undergraduate students Connor Davel and Jashan Chopra received
550 financial support from the University of Colorado Boulder's Undergraduate Research
551 Opportunities Program (UROP; grant nos. 7245334 and 5269631, respectively). Support for most
552 CIRES employees is from NOAA award no. NA17OAR4320101. ATom was funded by NASA
553 ROSES-2013 NRA NNH13ZDA001N-EVS2.

554

555 **References**

556 Allen, H. M., Crouse, J. D., Kim, M. J., Teng, A. P., and Wennberg, P. O.: Atmospheric Tomography Mission
557 (ATom)ATom: L2 In Situ Data from Caltech Chemical Ionization Mass Spectrometer (CIT-CIMS), 79.481444 MB,
558 <https://doi.org/10.3334/ORN LDAAC/1713>, 2019.

559 Alvarez, R. A., Zavala-Araiza, D., Lyon, D. R., Allen, D. T., Barkley, Z. R., Brandt, A. R., Davis, K. J., Herndon, S.
560 C., Jacob, D. J., Karion, A., Kort, E. A., Lamb, B. K., Lauvaux, T., Maasakkers, J. D., Marchese, A. J., Omara, M.,
561 Pacala, S. W., Peischl, J., Robinson, A. L., Shepson, P. B., Sweeney, C., Townsend-Small, A., Wofsy, S. C., and
562 Hamburg, S. P.: Assessment of methane emissions from the U.S. oil and gas supply chain, 361, 186–188,
563 <https://doi.org/10.1126/science.aar7204>, 2018.

564 Andreae, M. O.: Emission of trace gases and aerosols from biomass burning – an updated assessment, 19, 8523–8546,
565 <https://doi.org/10.5194/acp-19-8523-2019>, 2019.

566 Angot, H., Helmig, D., Hueber, J., Chopra, J., Davel, C., and Wiedinmyer, C.: Atmospheric tracers for Arctic wildfires,
567 air pollution, atmospheric chemistry, and climate change at GEOSummit, Greenland, since 2018,
568 <https://doi.org/10.18739/A2FX73Z7B>, 2020.

569 Aydin, M., Verhulst, K. R., Saltzman, E. S., Battle, M. O., Montzka, S. A., Blake, D. R., Tang, Q., and Prather, M. J.:
570 Recent decreases in fossil-fuel emissions of ethane and methane derived from firm air, *Nature*, 476, 198–201,
571 <https://doi.org/10.1038/nature10352>, 2011.

572 Barletta, B., Biggs, B. C., Blake, D. R., Blake, N., Hoffman, A., Hughes, S., Meinardi, S., Vizenor, N., and Woods,
573 C. T.: ATom: L2 Halocarbons and Hydrocarbons from the UC-Irvine Whole Air Sampler (WAS),
574 <https://doi.org/10.3334/ORN LDAAC/1751>, 2020.

575 Barrie, L. A., Gregor, D., Hargrave, B., Lake, R., Muir, D., Shearer, R., Tracey, B., and Bidleman, T.: Arctic
576 contaminants: sources, occurrence and pathways, *Science of The Total Environment*, 122, 1–74,
577 [https://doi.org/10.1016/0048-9697\(92\)90245-N](https://doi.org/10.1016/0048-9697(92)90245-N), 1992.

578 Becker, S., Halsall, C. J., Tych, W., Kallenborn, R., Su, Y., and Hung, H.: Long-term trends in atmospheric
579 concentrations of α - and γ -HCH in the Arctic provide insight into the effects of legislation and climatic fluctuations
580 on contaminant levels, *Atmospheric Environment*, 42, 8225–8233, <https://doi.org/10.1016/j.atmosenv.2008.07.058>,
581 2008.

582 Bondur, V. G., Mokhov, I. I., Voronova, O. S., and Sitnov, S. A.: Satellite Monitoring of Siberian Wildfires and Their
583 Effects: Features of 2019 Anomalies and Trends of 20-Year Changes, *Dokl. Earth Sc.*, 492, 370–375,
584 <https://doi.org/10.1134/S1028334X20050049>, 2020.

585 Bourgeois, I., Peischl, J., Neuman, A., Brown, S., Thompson, C., Aikin, K. C., Allen, H. M., Angot, H., Apel, E. C.,
586 Baublitz, C. B., Brewer, J., Campuzano-Jost, P., Commane, R., Crouse, J. D., Daube, B. C., DiGangi, J. P., Diskin,
587 G. S., Emmons, L. K., Fiore, A. M., Gkatzelis, G. I., Hills, A., Hornbrook, R. S., Huey, L. G., Kim, M., Lacey, F.,
588 McKain, L. T., Nault, B. A., Parrish, D. D., Ray, E., Sweeney, C., Tanner, D., Wofsy, S. C., and Ryerson, T. B.: Large
589 contribution of biomass burning emissions to ozone throughout the global remote troposphere, in review.

590 Brenninkmeijer, C. A. M., Manning, M. R., Lowe, D. C., Wallace, G., Sparks, R. J., and Volz-Thomas, A.:
591 Interhemispheric asymmetry in OH abundance inferred from measurements of atmospheric 14 CO, 356, 50–52,
592 <https://doi.org/10.1038/356050a0>, 1992.

593 Caporin, M. and Fontini, F.: The long-run oil–natural gas price relationship and the shale gas revolution, *Energy*
594 *Economics*, 64, 511–519, <https://doi.org/10.1016/j.eneco.2016.07.024>, 2017.

595 Carslaw, D. and Ropkins, K.: openair - An R package for air quality data analysis, *Environ Modell Softw*, 27–28, 52–
596 61, <https://doi.org/10.1016/j.envsoft.2011.09.008>, 2012.

597 Chameides, W. L. and Cicerone, R. J.: EFFECTS OF NONMETHANE HYDROCARBONS IN THE
598 ATMOSPHERE., 83, 947–952, <https://doi.org/10.1029/JC083iC02p00947>, 1978.

599 Dalsøren, S. B., Myhre, G., Hodnebrog, Ø., Myhre, C. L., Stohl, A., Pisso, I., Schwietzke, S., Höglund-Isaksson, L.,
600 Helmig, D., Reimann, S., Sauvage, S., Schmidbauer, N., Read, K. A., Carpenter, L. J., Lewis, A. C., Punjabi, S., and
601 Wallasch, M.: Discrepancy between simulated and observed ethane and propane levels explained by underestimated
602 fossil emissions, 11, 178–184, <https://doi.org/10.1038/s41561-018-0073-0>, 2018.

603 Dlugokencky, E. J., Steele, L. P., Lang, P. M., and Masarie, K. A.: The growth rate and distribution of atmospheric
604 methane, 99, 17021–17043, <https://doi.org/10.1029/94JD01245>, 1994.

605 Dlugokencky, E. J., Masarie, K. A., Tans, P. P., Conway, T. J., and Xiong, X.: Is the amplitude of the methane seasonal
606 cycle changing?, *Atmospheric Environment*, 31, 21–26, [https://doi.org/10.1016/S1352-2310\(96\)00174-4](https://doi.org/10.1016/S1352-2310(96)00174-4), 1997.

607 Draxler, R. R. and Rolph, G. D.: HYSPLIT (HYbrid Single-Particle Lagrangian Integrated Trajectory) Model access
608 via NOAA ARL READY Website (<http://www.arl.noaa.gov/HYSPLIT.php>), last access: 24 October 2015. NOAA
609 Air Resources Laboratory, College Park, MD., 2013.

610 Duncan, B. N. and Bey, I.: A modeling study of the export pathways of pollution from Europe: Seasonal and
611 interannual variations (1987-1997), 109, D08301, <https://doi.org/10.1029/2003JD004079>, 2004.

612 Eckhardt, S., Stohl, A., Beirle, S., Spichtinger, N., James, P., Forster, C., Junker, C., Wagner, T., Platt, U., and
613 Jennings, S. G.: The North Atlantic Oscillation controls air pollution transport to the Arctic, 3, 1769–1778,
614 <https://doi.org/10.5194/acp-3-1769-2003>, 2003.

615 Feng, G.-F., Wang, Q.-J., Chu, Y., Wen, J., and Chang, C.-P.: Does the shale gas boom change the natural gas price-
616 production relationship? Evidence from the U.S. market, *Energy Economics*, 104327,
617 <https://doi.org/10.1016/j.eneco.2019.03.001>, 2019.

618 Franco, B., Bader, W., Toon, G. C., Bray, C., Perrin, A., Fischer, E. V., Sudo, K., Boone, C. D., Bovy, B., Lejeune,
619 B., Servais, C., and Mahieu, E.: Retrieval of ethane from ground-based FTIR solar spectra using improved
620 spectroscopy: Recent burden increase above Jungfraujoch, *Journal of Quantitative Spectroscopy and Radiative*
621 *Transfer*, 160, 36–49, <https://doi.org/10.1016/j.jqsrt.2015.03.017>, 2015.

622 Franco, B., Mahieu, E., Emmons, L. K., Tzompa-Sosa, Z. A., Fischer, E. V., Sudo, K., Bovy, B., Conway, S., Griffin,
623 D., Hannigan, J. W., Strong, K., and Walker, K. A.: Evaluating ethane and methane emissions associated with the
624 development of oil and natural gas extraction in North America, *Environ. Res. Lett.*, 11, 044010,
625 <https://doi.org/10.1088/1748-9326/11/4/044010>, 2016.

626 Geller, L. S., Elkins, J. W., Lobert, J. M., Clarke, A. D., Hurst, D. F., Butler, J. H., and Myers, R. C.: Tropospheric
627 SF₆: Observed latitudinal distribution and trends, derived emissions and interhemispheric exchange time, 24, 675–
628 678, <https://doi.org/10.1029/97GL00523>, 1997.

629 Gettelman, A., Mills, M. J., Kinnison, D. E., Garcia, R. R., Smith, A. K., Marsh, D. R., Tilmes, S., Vitt, F., Bardeen,
630 C. G., McInerny, J., Liu, H.-L., Solomon, S. C., Polvani, L. M., Emmons, L. K., Lamarque, J.-F., Richter, J. H.,
631 Glanville, A. S., Bacmeister, J. T., Phillips, A. S., Neale, R. B., Simpson, I. R., DuVivier, A. K., Hodzic, A., and
632 Randel, W. J.: The Whole Atmosphere Community Climate Model Version 6 (WACCM6), 124, 12380–12403,
633 <https://doi.org/10.1029/2019JD030943>, 2019.

634 Goldstein, A. H., Wofsy, S. C., and Spivakovsky, C. M.: Seasonal variations of nonmethane hydrocarbons in rural
635 New England: Constraints on OH concentrations in northern midlatitudes, 100, 21023–21033,
636 <https://doi.org/10.1029/95JD02034>, 1995.

- 637 Gong, B.: The Development and Implication of Nature Gas Market in the Context of the Shale Revolution, in: Shale
638 Energy Revolution: The Rise and Fall of Global Oil and Gas Industry, edited by: Gong, B., Springer, Singapore, 19–
639 36, https://doi.org/10.1007/978-981-15-4855-0_2, 2020.
- 640 Guenther, A. B., Jiang, X., Heald, C. L., Sakulyanontvittaya, T., Duhl, T., Emmons, L. K., and Wang, X.: The Model
641 of Emissions of Gases and Aerosols from Nature version 2.1 (MEGAN2.1): an extended and updated framework for
642 modeling biogenic emissions, 5, 1471–1492, <https://doi.org/10.5194/gmd-5-1471-2012>, 2012.
- 643 Gvakharia, A., Kort, E. A., Brandt, A., Peischl, J., Ryerson, T. B., Schwarz, J. P., Smith, M. L., and Sweeney, C.:
644 Methane, Black Carbon, and Ethane Emissions from Natural Gas Flares in the Bakken Shale, North Dakota, Environ.
645 Sci. Technol., 51, 5317–5325, <https://doi.org/10.1021/acs.est.6b05183>, 2017.
- 646 Hartery, S., Commane, R., Lindaas, J., Sweeney, C., Henderson, J., Mountain, M., Steiner, N., McDonald, K., Dinardo,
647 S. J., Miller, C. E., Wofsy, S. C., and Chang, R. Y.-W.: Estimating regional-scale methane flux and budgets using
648 CARVE aircraft measurements over Alaska, 18, 185–202, <https://doi.org/10.5194/acp-18-185-2018>, 2018.
- 649 Hausmann, P., Sussmann, R., and Smale, D.: Contribution of oil and natural gas production to renewed increase in
650 atmospheric methane (2007–2014): top–down estimate from ethane and methane column observations, 16, 3227–
651 3244, <https://doi.org/10.5194/acp-16-3227-2016>, 2016.
- 652 Helmig, D.: Atmospheric hydrocarbons as tracers for climate change, air transport, and oxidation chemistry in the
653 Arctic, GEOSummit, Greenland, 2008–2017., <https://doi.org/10.18739/A2RS0X>, 2017.
- 654 Helmig, D., Bottenheim, J., Galbally, I. E., Lewis, A., Milton, M. J. T., Penkett, S., Plass-Duelmer, C., Reimann, S.,
655 Tans, P., and Thiel, S.: Volatile Organic Compounds in the Global Atmosphere, 90, 513–514,
656 <https://doi.org/10.1029/2009EO520001>, 2009.
- 657 Helmig, D., Petrenko, V., Martinerie, P., Witrant, E., Röckmann, T., Zuiderweg, A., Holzinger, R., Hueber, J.,
658 Thompson, C., White, J. W. C., Sturges, W., Baker, A., Blunier, T., Etheridge, D., Rubino, M., and Tans, P.:
659 Reconstruction of Northern Hemisphere 1950–2010 atmospheric non-methane hydrocarbons, 14, 1463–1483,
660 <https://doi.org/10.5194/acp-14-1463-2014>, 2014.
- 661 Helmig, D., Rossabi, S., Hueber, J., Tans, P., Montzka, S. A., Masarie, K., Thoning, K., Plass-Duelmer, C., Claude,
662 A., Carpenter, L. J., Lewis, A. C., Punjabi, S., Reimann, S., Vollmer, M. K., Steinbrecher, R., Hannigan, J. W.,
663 Emmons, L. K., Mahieu, E., Franco, B., Smale, D., and Pozzer, A.: Reversal of global atmospheric ethane and propane
664 trends largely due to US oil and natural gas production, 9, 490–495, <https://doi.org/10.1038/ngeo2721>, 2016.
- 665 Hirdman, D., Sodemann, H., Eckhardt, S., Burkhardt, J. F., Jefferson, A., Mefford, T., Quinn, P. K., Sharma, S., Ström,
666 J., and Stohl, A.: Source identification of short-lived air pollutants in the Arctic using statistical analysis of
667 measurement data and particle dispersion model output, 10, 669–693, <https://doi.org/10.5194/acp-10-669-2010>, 2010.
- 668 Houweling, S., Dentener, F., and Lelieveld, J.: The impact of nonmethane hydrocarbon compounds on tropospheric
669 photochemistry, 103, 10673–10696, <https://doi.org/10.1029/97JD03582>, 1998.
- 670 Hu, Q. and Feng, S.: Influence of the Arctic oscillation on central United States summer rainfall, 115,
671 <https://doi.org/10.1029/2009JD011805>, 2010.
- 672 Iversen, T. and Joranger, E.: Arctic air pollution and large scale atmospheric flows, Atmospheric Environment (1967),
673 19, 2099–2108, [https://doi.org/10.1016/0004-6981\(85\)90117-9](https://doi.org/10.1016/0004-6981(85)90117-9), 1985.
- 674 Jacob, D. J., Crawford, J. H., Maring, H., Clarke, A. D., Dibb, J. E., Emmons, L. K., Ferrare, R. A., Hostetler, C. A.,
675 Russell, P. B., Singh, H. B., Thompson, A. M., Shaw, G. E., McCauley, E., Pederson, J. R., and Fisher, J. A.: The
676 Arctic Research of the Composition of the Troposphere from Aircraft and Satellites (ARCTAS) mission: design,
677 execution, and first results, 10, 5191–5212, <https://doi.org/10.5194/acp-10-5191-2010>, 2010.

678 Janssens-Maenhout, G., Crippa, M., Guizzardi, D., Dentener, F., Muntean, M., Pouliot, G., Keating, T., Zhang, Q.,
679 Kurokawa, J., Wankmüller, R., Denier van der Gon, H., Kuenen, J. J. P., Klimont, Z., Frost, G., Darras, S., Koffi, B.,
680 and Li, M.: HTAP_v2.2: a mosaic of regional and global emission grid maps for 2008 and 2010 to study hemispheric
681 transport of air pollution, 15, 11411–11432, <https://doi.org/10.5194/acp-15-11411-2015>, 2015.

682 Kahl, J. D. W., Martinez, D. A., Kuhns, H., Davidson, C. I., Jaffrezo, J.-L., and Harris, J. M.: Air mass trajectories to
683 Summit, Greenland: A 44-year climatology and some episodic events, 102, 26861–26875,
684 <https://doi.org/10.1029/97JC00296>, 1997.

685 Komhyr, W. D., Gammon, R. H., Harris, T. B., Waterman, L. S., Conway, T. J., Taylor, W. R., and Thoning, K. W.:
686 Global atmospheric CO₂ distribution and variations from 1968–1982 NOAA/GMCC CO₂ flask sample data, 90,
687 5567–5596, <https://doi.org/10.1029/JD090iD03p05567>, 1985.

688 Kort, E. A., Smith, M. L., Murray, L. T., Gvakharia, A., Brandt, A. R., Peischl, J., Ryerson, T. B., Sweeney, C., and
689 Travis, K.: Fugitive emissions from the Bakken shale illustrate role of shale production in global ethane shift, 43,
690 4617–4623, <https://doi.org/10.1002/2016GL068703>, 2016.

691 Kramer, L. J., Helmig, D., Burkhardt, J. F., Stohl, A., Oltmans, S., and Honrath, R. E.: Seasonal variability of
692 atmospheric nitrogen oxides and non-methane hydrocarbons at the GEOSummit station, Greenland, 15, 6827–6849,
693 <https://doi.org/10.5194/acp-15-6827-2015>, 2015.

694 Lassman, W., Ford, B., Gan, R. W., Pfister, G., Magzamen, S., Fischer, E. V., and Pierce, J. R.: Spatial and temporal
695 estimates of population exposure to wildfire smoke during the Washington state 2012 wildfire season using blended
696 model, satellite, and in situ data, 1, 106–121, <https://doi.org/10.1002/2017GH000049>, 2017.

697 Law, K. S., Stohl, A., Quinn, P. K., Brock, C., Burkhardt, J., Paris, J.-D., Ancellet, G., Singh, H. B., Roiger, A.,
698 Schlager, H., Dibb, J., Jacob, D. J., Arnold, S. R., Pelon, J., and Thomas, J. L.: Arctic Air Pollution: New Insights
699 from POLARCAT-IPY, <https://doi.org/10.1175/BAMS-D-13-00017.1>, 2014.

700 Lelieveld, J., Dentener, F. J., Peters, W., and Krol, M. C.: On the role of hydroxyl radicals in the self-cleansing capacity
701 of the troposphere, 4, 2337–2344, <https://doi.org/10.5194/acp-4-2337-2004>, 2004.

702 Levy, H.: Normal Atmosphere: Large Radical and Formaldehyde Concentrations Predicted, 173, 141–143,
703 <https://doi.org/10.1126/science.173.3992.141>, 1971.

704 Logan, J. A., Prather, M. J., Wofsy, S. C., and McElroy, M. B.: Tropospheric chemistry: A global perspective, 86,
705 7210–7254, <https://doi.org/10.1029/JC086iC08p07210>, 1981.

706 Masarie, K. A. and Tans, P. P.: Extension and integration of atmospheric carbon dioxide data into a globally consistent
707 measurement record, 100, 11593–11610, <https://doi.org/10.1029/95JD00859>, 1995.

708 Miller, B. R., Weiss, R. F., Salameh, P. K., Tanhua, T., Grealley, B. R., Mühle, J., and Simmonds, P. G.: Medusa: A
709 Sample Preconcentration and GC/MS Detector System for in Situ Measurements of Atmospheric Trace Halocarbons,
710 Hydrocarbons, and Sulfur Compounds, *Anal. Chem.*, 80, 1536–1545, <https://doi.org/10.1021/ac702084k>, 2008.

711 Miller, J. B., Mack, K. A., Dissly, R., White, J. W. C., Dlugokencky, E. J., and Tans, P. P.: Development of analytical
712 methods and measurements of ¹³C/¹²C in atmospheric CH₄ from the NOAA Climate Monitoring and Diagnostics
713 Laboratory Global Air Sampling Network, 107, ACH 11-1-ACH 11-15, <https://doi.org/10.1029/2001JD000630>, 2002.

714 Montzka, S. A., Dutton, G. S., Yu, P., Ray, E., Portmann, R. W., Daniel, J. S., Kuijpers, L., Hall, B. D., Mondeel, D.,
715 Siso, C., Nance, J. D., Rigby, M., Manning, A. J., Hu, L., Moore, F., Miller, B. R., and Elkins, J. W.: An unexpected
716 and persistent increase in global emissions of ozone-depleting CFC-11, 557, 413–417, <https://doi.org/10.1038/s41586-018-0106-2>, 2018.

718 Naik, V., Voulgarakis, A., Fiore, A. M., Horowitz, L. W., Lamarque, J.-F., Lin, M., Prather, M. J., Young, P. J.,
719 Bergmann, D., Cameron-Smith, P. J., Cionni, I., Collins, W. J., Dalsøren, S. B., Doherty, R., Eyring, V., Faluvegi, G.,
720 Folberth, G. A., Josse, B., Lee, Y. H., MacKenzie, I. A., Nagashima, T., van Noije, T. P. C., Plummer, D. A., Righi,
721 M., Rumbold, S. T., Skeie, R., Shindell, D. T., Stevenson, D. S., Strode, S., Sudo, K., Szopa, S., and Zeng, G.:
722 Preindustrial to present-day changes in tropospheric hydroxyl radical and methane lifetime from the Atmospheric
723 Chemistry and Climate Model Intercomparison Project (ACCMIP), 13, 5277–5298, <https://doi.org/10.5194/acp-13-5277-2013>, 2013.

725 Naus, S., Montzka, S. A., Patra, P. K., and Krol, M. C.: A 3D-model inversion of methyl chloroform to constrain the
726 atmospheric oxidative capacity, 1–23, <https://doi.org/10.5194/acp-2020-624>, 2020.

727 Nicewonger, M. R., Aydin, M., Prather, M. J., and Saltzman, E. S.: Extracting a History of Global Fire Emissions for
728 the Past Millennium From Ice Core Records of Acetylene, Ethane, and Methane, 125, e2020JD032932,
729 <https://doi.org/10.1029/2020JD032932>, 2020.

730 Nisbet, E. G., Dlugokencky, E. J., and Bousquet, P.: Methane on the Rise—Again, 343, 493–495,
731 <https://doi.org/10.1126/science.1247828>, 2014.

732 Nisbet, E. G., Manning, M. R., Dlugokencky, E. J., Fisher, R. E., Lowry, D., Michel, S. E., Myhre, C. L., Platt, S. M.,
733 Allen, G., Bousquet, P., Brownlow, R., Cain, M., France, J. L., Hermansen, O., Hossaini, R., Jones, A. E., Levin, I.,
734 Manning, A. C., Myhre, G., Pyle, J. A., Vaughn, B. H., Warwick, N. J., and White, J. W. C.: Very Strong Atmospheric
735 Methane Growth in the 4 Years 2014–2017: Implications for the Paris Agreement, 33, 318–342,
736 <https://doi.org/10.1029/2018GB006009>, 2019.

737 Octaviani, M., Stemmler, I., Lammel, G., and Graf, H. F.: Atmospheric Transport of Persistent Organic Pollutants to
738 and from the Arctic under Present-Day and Future Climate, *Environ. Sci. Technol.*, 49, 3593–3602,
739 <https://doi.org/10.1021/es505636g>, 2015.

740 Oltmans, S. J., Cheadle, L. C., Helmig, D., Angot, H., Pétron, G., Montzka, S. A., Dlugokencky, E. J., Miller, B., Hall,
741 B., Schnell, R. C., Kofler, J., Wolter, S., Crotwell, M., Siso, C., Tans, P., and Andrews, A.: Atmospheric oil and
742 natural gas hydrocarbon trends in the Northern Colorado Front Range are notably smaller than inventory emissions
743 reductions, *Elementa: Science of the Anthropocene*, 9, <https://doi.org/10.1525/elementa.2020.00136>, 2021.

744 Pekney, N. J., Davidson, C. I., Zhou, L., and Hopke, P. K.: Application of PSCF and CPF to PMF-Modeled Sources
745 of PM_{2.5} in Pittsburgh, 40, 952–961, <https://doi.org/10.1080/02786820500543324>, 2006.

746 Perrone, M. G., Vratolis, S., Georgieva, E., Török, S., Šega, K., Veleva, B., Osán, J., Bešlić, I., Kertész, Z., Pernigotti,
747 D., Eleftheriadis, K., and Belis, C. A.: Sources and geographic origin of particulate matter in urban areas of the Danube
748 macro-region: The cases of Zagreb (Croatia), Budapest (Hungary) and Sofia (Bulgaria), *Sci Total Environ*, 619–620,
749 1515–1529, <https://doi.org/10.1016/j.scitotenv.2017.11.092>, 2018.

750 Pétron, G., Frost, G., Miller, B. R., Hirsch, A. I., Montzka, S. A., Karion, A., Trainer, M., Sweeney, C., Andrews, A.
751 E., Miller, L., Kofler, J., Bar-Ilan, A., Dlugokencky, E. J., Patrick, L., Moore, C. T., Ryerson, T. B., Siso, C., Kolodzey,
752 W., Lang, P. M., Conway, T., Novelli, P., Masarie, K., Hall, B., Guenther, D., Kitzi, D., Miller, J., Welsh, D., Wolfe,
753 D., Neff, W., and Tans, P.: Hydrocarbon emissions characterization in the Colorado Front Range: A pilot study, 117,
754 <https://doi.org/10.1029/2011JD016360>, 2012.

755 Pétron, G., Karion, A., Sweeney, C., Miller, B. R., Montzka, S. A., Frost, G. J., Trainer, M., Tans, P., Andrews, A.,
756 Kofler, J., Helmig, D., Guenther, D., Dlugokencky, E., Lang, P., Newberger, T., Wolter, S., Hall, B., Novelli, P.,
757 Brewer, A., Conley, S., Hardesty, M., Banta, R., White, A., Noone, D., Wolfe, D., and Schnell, R.: A new look at
758 methane and nonmethane hydrocarbon emissions from oil and natural gas operations in the Colorado Denver-
759 Julesburg Basin, 119, 6836–6852, <https://doi.org/10.1002/2013JD021272>, 2014.

760 G2401 Gas Concentration Analyzer | Picarro: https://www.picarro.com/products/g2401_gas_concentration_analyzer,
761 last access: 31 March 2020.

762 Pollmann, J., Helmig, D., Hueber, J., Plass-Dülmer, C., and Tans, P.: Sampling, storage, and analysis of C2–C7 non-
763 methane hydrocarbons from the US National Oceanic and Atmospheric Administration Cooperative Air Sampling
764 Network glass flasks, *Journal of Chromatography A*, 1188, 75–87, <https://doi.org/10.1016/j.chroma.2008.02.059>,
765 2008.

766 Arctic Oil & Gas Development: The Case of Greenland: [https://arcticyearbook.com/arctic-yearbook/2018/2018-](https://arcticyearbook.com/arctic-yearbook/2018/2018-scholarly-papers/285-arctic-oil-gas-development-the-case-of-greenland)
767 [scholarly-papers/285-arctic-oil-gas-development-the-case-of-greenland](https://arcticyearbook.com/arctic-yearbook/2018/2018-scholarly-papers/285-arctic-oil-gas-development-the-case-of-greenland), last access: 25 November 2020.

768 Pozzer, A., Pollmann, J., Taraborrelli, D., Jöckel, P., Helmig, D., Tans, P., Hueber, J., and Lelieveld, J.: Observed and
769 simulated global distribution and budget of atmospheric C2–C5 alkanes, 10, 4403–4422, [https://doi.org/10.5194/acp-](https://doi.org/10.5194/acp-10-4403-2010)
770 [10-4403-2010](https://doi.org/10.5194/acp-10-4403-2010), 2010.

771 Rex, D. F.: Blocking Action in the Middle Troposphere and its Effect upon Regional Climate, 2, 275–301,
772 <https://doi.org/10.1111/j.2153-3490.1950.tb00339.x>, 1950.

773 Greenland Opens Offshore Areas for Drilling:
774 https://www.rigzone.com/news/greenland_opens_offshore_areas_for_drilling-05-nov-2020-163772-article/, last
775 access: 25 November 2020.

776 Roest, G. and Schade, G.: Quantifying alkane emissions in the Eagle Ford Shale using boundary layer enhancement,
777 17, 11163–11176, <https://doi.org/10.5194/acp-17-11163-2017>, 2017.

778 Rudolph, J.: The tropospheric distribution and budget of ethane, 100, 11369–11381,
779 <https://doi.org/10.1029/95JD00693>, 1995.

780 Scanlon, J. T. and Willis, D. E.: Calculation of Flame Ionization Detector Relative Response Factors Using the
781 Effective Carbon Number Concept, *J Chromatogr Sci*, 23, 333–340, <https://doi.org/10.1093/chromsci/23.8.333>, 1985.

782 von Schneidemesser, E., Monks, P. S., and Plass-Duelmer, C.: Global comparison of VOC and CO observations in
783 urban areas, *Atmospheric Environment*, 44, 5053–5064, <https://doi.org/10.1016/j.atmosenv.2010.09.010>, 2010.

784 Schultz, M. G., Akimoto, H., Bottenheim, J., Buchmann, B., Galbally, I. E., Gilge, S., Helmig, D., Koide, H., Lewis,
785 A. C., Novelli, P. C., Dülmer, C. P., Ryerson, T. B., Steinbacher, M., Steinbrecher, R., Tarasova, O., Tørseth, K.,
786 Thouret, V., and Zellweger, C.: The Global Atmosphere Watch reactive gases measurement network, 3, 000067,
787 <https://doi.org/10.12952/journal.elementa.000067>, 2015.

788 Sicotte, D. M.: From cheap ethane to a plastic planet: Regulating an industrial global production network, *Energy*
789 *Research & Social Science*, 66, 101479, <https://doi.org/10.1016/j.erss.2020.101479>, 2020.

790 Simpson, I. J., Andersen, M. P. S., Meinardi, S., Bruhwiler, L., Blake, N. J., Helmig, D., Rowland, F. S., and Blake,
791 D. R.: Long-term decline of global atmospheric ethane concentrations and implications for methane, *Nature*, 488,
792 490–494, <https://doi.org/10.1038/nature11342>, 2012.

793 Spivakovsky, C. M., Logan, J. A., Montzka, S. A., Balkanski, Y. J., Foreman-Fowler, M., Jones, D. B. A., Horowitz,
794 L. W., Fusco, A. C., Brenninkmeijer, C. a. M., Prather, M. J., Wofsy, S. C., and McElroy, M. B.: Three-dimensional
795 climatological distribution of tropospheric OH: Update and evaluation, 105, 8931–8980,
796 <https://doi.org/10.1029/1999JD901006>, 2000.

797 Steele, L. P.: Atmospheric Methane Concentrations, the NOAA/CMDL Global Cooperative Flask Sampling Network,
798 1983–1988, Oak Ridge National Laboratory, 324 pp., 1991.

799 Steele, L. P., Fraser, P. J., Rasmussen, R. A., Khalil, M. A. K., Conway, T. J., Crawford, A. J., Gammon, R. H.,
800 Masarie, K. A., and Thoning, K. W.: The global distribution of methane in the troposphere, *J Atmos Chem*, 5, 125–
801 171, <https://doi.org/10.1007/BF00048857>, 1987.

802 Tanner, D., Helmig, D., Hueber, J., and Goldan, P.: Gas chromatography system for the automated, unattended, and
803 cryogen-free monitoring of C₂ to C₆ non-methane hydrocarbons in the remote troposphere, *Journal of*
804 *Chromatography A*, 1111, 76–88, <https://doi.org/10.1016/j.chroma.2006.01.100>, 2006.

805 Thompson, A. M.: The Oxidizing Capacity of the Earth’s Atmosphere: Probable Past and Future Changes, 256, 1157–
806 1165, <https://doi.org/10.1126/science.256.5060.1157>, 1992.

807 Thoning, K. W., Tans, P. P., and Komhyr, W. D.: Atmospheric carbon dioxide at Mauna Loa Observatory: 2. Analysis
808 of the NOAA GMCC data, 1974–1985, 94, 8549–8565, <https://doi.org/10.1029/JD094iD06p08549>, 1989.

809 Trolier, M., White, J. W. C., Tans, P. P., Masarie, K. A., and Gemery, P. A.: Monitoring the isotopic composition of
810 atmospheric CO₂: Measurements from the NOAA Global Air Sampling Network, 101, 25897–25916,
811 <https://doi.org/10.1029/96JD02363>, 1996.

812 Tzompa-Sosa, Z. A., Mahieu, E., Franco, B., Keller, C. A., Turner, A. J., Helmig, D., Fried, A., Richter, D., Weibring,
813 P., Walega, J., Yacovitch, T. I., Herndon, S. C., Blake, D. R., Hase, F., Hannigan, J. W., Conway, S., Strong, K.,
814 Schneider, M., and Fischer, E. V.: Revisiting global fossil fuel and biofuel emissions of ethane, 122, 2493–2512,
815 <https://doi.org/10.1002/2016JD025767>, 2017.

816 Tzompa-Sosa, Z. A., Henderson, B. H., Keller, C. A., Travis, K., Mahieu, E., Franco, B., Estes, M., Helmig, D., Fried,
817 A., Richter, D., Weibring, P., Walega, J., Blake, D. R., Hannigan, J. W., Ortega, I., Conway, S., Strong, K., and
818 Fischer, E. V.: Atmospheric Implications of Large C₂-C₅ Alkane Emissions From the U.S. Oil and Gas Industry, 124,
819 1148–1169, <https://doi.org/10.1029/2018JD028955>, 2019.

820 U.S. Field Production of Natural Gas Liquids:
821 https://www.eia.gov/dnav/pet/hist/LeafHandler.ashx?n=PET&s=M_EPL2_FPF_NUS_MBBLD&f=A, last access: 8
822 March 2021.

823 U.S. Field Production of Propane:
824 https://www.eia.gov/dnav/pet/hist/LeafHandler.ashx?n=PET&s=M_EPLLPA_FPF_NUS_MBBL&f=M, last access:
825 8 March 2021.

826 Val Martin, M., Heald, C. L., Ford, B., Prenni, A. J., and Wiedinmyer, C.: A decadal satellite analysis of the origins
827 and impacts of smoke in Colorado, 2013.

828 Warneke, C., Gouw, J. A. de, Holloway, J. S., Peischl, J., Ryerson, T. B., Atlas, E., Blake, D., Trainer, M., and Parrish,
829 D. D.: Multiyear trends in volatile organic compounds in Los Angeles, California: Five decades of decreasing
830 emissions, 117, <https://doi.org/10.1029/2012JD017899>, 2012.

831 Warner, M. S. C.: Introduction to PySPLIT: A Python Toolkit for NOAA ARL’s HYSPLIT Model, 20, 47–62,
832 <https://doi.org/10.1109/MCSE.2017.3301549>, 2018.

833 Wiedinmyer, C., Akagi, S. K., Yokelson, R. J., Emmons, L. K., Al-Saadi, J. A., Orlando, J. J., and Soja, A. J.: The
834 Fire INventory from NCAR (FINN): a high resolution global model to estimate the emissions from open burning, 4,
835 625–641, <https://doi.org/10.5194/gmd-4-625-2011>, 2011.

836 Wiedinmyer, C., Kumra, Y., McDonald-Buller, E. C., Seto, K., Emmons, L. K., Buccholz, R., Tang, W., Joseph, M.,
837 Barsanti, K., Carlton, A. M., and Yokelson, R. J.: The Fire Inventory from NCAR version 2: an updated global fire
838 emissions model for climate and chemistry applications., *Journal of Advances in Modeling Earth Systems*, in prep.

839 WMO: GAW Report, 171. A WMO/GAW Expert Workshop on Global Long-term Measurements of Volatile Organic
840 Compounds, WMO, Geneva, 36 p. pp., 2007.

841 Wofsy, S. C., Afshar, S., Allen, H. M., Apel, E. C., Asher, E. C., Barletta, B., Bent, J., Bian, H., Biggs, B. C., Blake,
842 D. R., Blake, N., Bourgeois, I., Brock, C. A., Brune, W. H., Budney, J. W., Bui, T. P., Butler, A., Campuzano-Jost,

843 P., Chang, C. S., Chin, M., Commane, R., Correa, G., Crouse, J. D., Cullis, P. D., Daube, B. C., Day, D. A., Dean-
844 Day, J. M., Dibb, J. E., Digangi, J. P., Diskin, G. S., Dollner, M., Elkins, J. W., Erdesz, F., Fiore, A. M., Flynn, C. M.,
845 Froyd, K. D., Gesler, D. W., Hall, S. R., Hanisco, T. F., Hannun, R. A., Hills, A. J., Hints, E. J., Hoffman, A.,
846 Hornbrook, R. S., Huey, L. G., Hughes, S., Jimenez, J. L., Johnson, B. J., Katich, J. M., Keeling, R. F., Kim, M. J.,
847 Kupc, A., Lait, L. R., Lamarque, J.-F., Liu, J., Mckain, K., Mclaughlin, R. J., Meinardi, S., Miller, D. O., Montzka, S.
848 A., Moore, F. L., Morgan, E. J., Murphy, D. M., Murray, L. T., Nault, B. A., Neuman, J. A., Newman, P. A., Nicely,
849 J. M., Pan, X., Paplawsky, W., Peischl, J., Prather, M. J., Price, D. J., Ray, E. A., Reeves, J. M., Richardson, M.,
850 Rollins, A. W., Rosenlof, K. H., Ryerson, T. B., Scheuer, E., Schill, G. P., Schroder, J. C., Schwarz, J. P., St. Clair, J.
851 M., Steenrod, S. D., Stephens, B. B., Strode, S. A., Sweeney, C., Tanner, D., Teng, A. P., Thames, A. B., Thompson,
852 C. R., Ullmann, K., Veres, P. R., Vizenor, N., Wagner, N. L., Watt, A., Weber, R., Weinzierl, B., et al.: ATom: Merged
853 Atmospheric Chemistry, Trace Gases, and Aerosols, <https://doi.org/10.3334/ORNLDAAAC/1581>, 2018.

854 Worton, D. R., Sturges, W. T., Reeves, C. E., Newland, M. J., Penkett, S. A., Atlas, E., Stroud, V., Johnson, K.,
855 Schmidbauer, N., Solberg, S., Schwander, J., and Barnola, J.-M.: Evidence from firm air for recent decreases in non-
856 methane hydrocarbons and a 20th century increase in nitrogen oxides in the northern hemisphere, *Atmospheric*
857 *Environment*, 54, 592–602, <https://doi.org/10.1016/j.atmosenv.2012.02.084>, 2012.

858 Xiao, Y., Logan, J. A., Jacob, D. J., Hudman, R. C., Yantosca, R., and Blake, D. R.: Global budget of ethane and
859 regional constraints on U.S. sources, 113, <https://doi.org/10.1029/2007JD009415>, 2008.

860 Yu, Y., Hung, H., Alexandrou, N., Roach, P., and Nordin, K.: Multiyear Measurements of Flame Retardants and
861 Organochlorine Pesticides in Air in Canada's Western Sub-Arctic, *Environ. Sci. Technol.*, 49, 8623–8630,
862 <https://doi.org/10.1021/acs.est.5b01996>, 2015.

863 Zhou, H., Hopke, P. K., Zhou, C., and Holsen, T. M.: Ambient mercury source identifications at a New York State
864 urban site: Rochester, NY, *Science of The Total Environment*, <https://doi.org/10.1016/j.scitotenv.2018.09.040>, 2018.

865 Zong, Z., Wang, X., Tian, C., Chen, Y., Fu, S., Qu, L., Ji, L., Li, J., and Zhang, G.: PMF and PSCF based source
866 apportionment of PM_{2.5} at a regional background site in North China, *Atmospheric Research*, 203, 207–215,
867 <https://doi.org/10.1016/j.atmosres.2017.12.013>, 2018.

868

Table 1: Rates of change and 95 % confidence interval (in brackets) inferred from discrete flask sampling (in ppt per year). ALT, BRW, MHD, LEF, and KUM refer to Alert, Utqiagvik/Barrow, Mace Head, Park Falls, and Cape Kumukahi. The localization of the sites can be found in Figure 1. The symbols shown next to each rate of change relate to how statistically significant the estimate is: $p < 0.001 = ***$, $p < 0.01 = **$, and $p < 0.05 = *$.

Site	2010-2014	2015-2018
Ethane		
ALT	+52.8 [+32.7, +73.0] ***	-56.9 [-79.9, -36.6] ***
BRW	+40.5 [+25.9, +59.1] ***	-50.6 [-69.4, -27.6] ***
KUM	+18.4 [+7.9, +29.5] ***	-43.1 [-62.1, -28.1] ***
LEF	+167.7 [+157.5, +186.0] ***	-247.8 [-312.2, -158.2] ***
MHD	+51.8 [+44.4, +63.2] ***	-18.6 [-102.6, +45.4]
Propane		
ALT	+24.8 [+16.5, +37.7] ***	-55.6 [-65.1, -45.9] ***
BRW	+14.5 [+9.1, +20.2] ***	-35.1 [-45.3, -25.6] ***
KUM	+3.1 [+0.2, +5.9] *	-13.2 [-15.9, -10.7] ***
LEF	+89.8 [+68.5, +123.5] ***	-110.0 [-173.6, -75.6] ***
MHD	+21.3 [+16.9, +27.1] ***	-24.2 [-56.2, -7.2] **



Figure 1: Location of the Greenland Environmental Observatory at Summit station (red dot, SUM) where long-term in-situ monitoring was carried out, and of Alert (ALT), Utqiagvik (formerly known as Barrow (BRW)), Mace Head (MHD), Park Falls (LEF), and Cape Kumukahi (KUM) where discrete samples were collected by both the NOAA/ESRL/GML CCGG and HATS flask sampling programs. The map is centered over the North Pole.

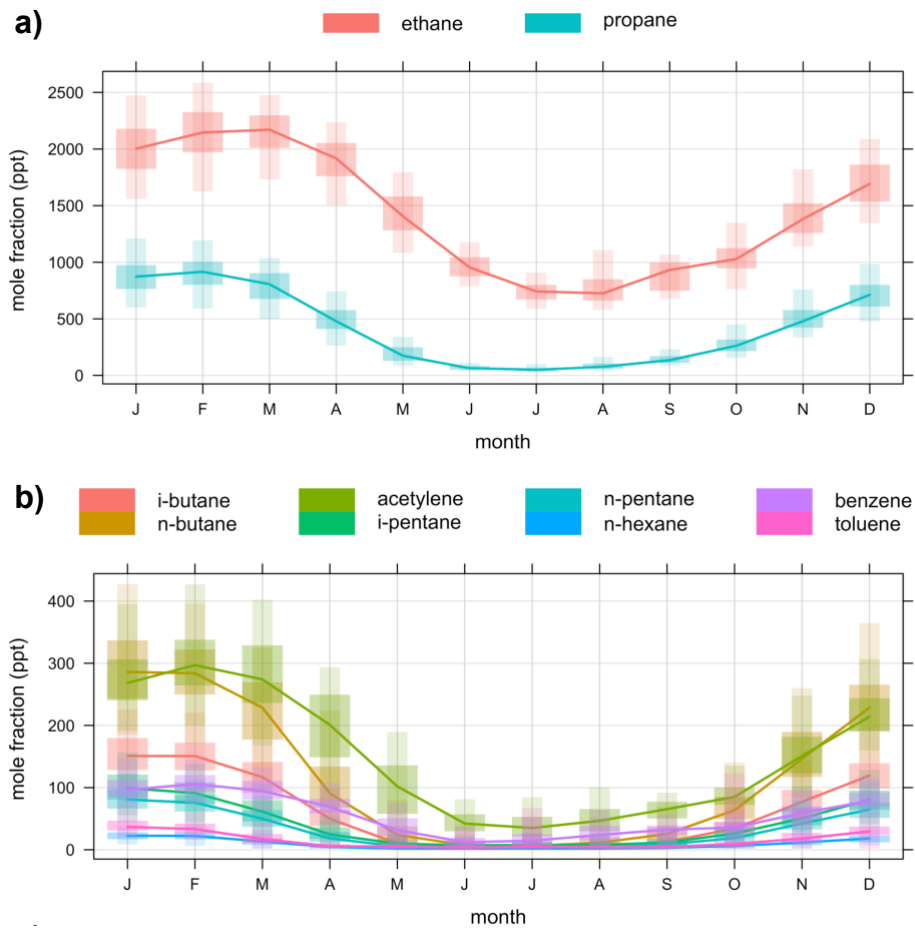


Figure 2: Monthly variation of **a)** ethane and propane, and **b)** C₄-C₇ non-methane hydrocarbons measured in ambient air at GEOSummit as inferred from 2008-2010 and 2012-2020 in-situ measurements. In the monthly boxplots, the lower and upper end of the box correspond to the 25th and 75th percentiles while the whiskers extend from the 5th to the 95th percentiles.

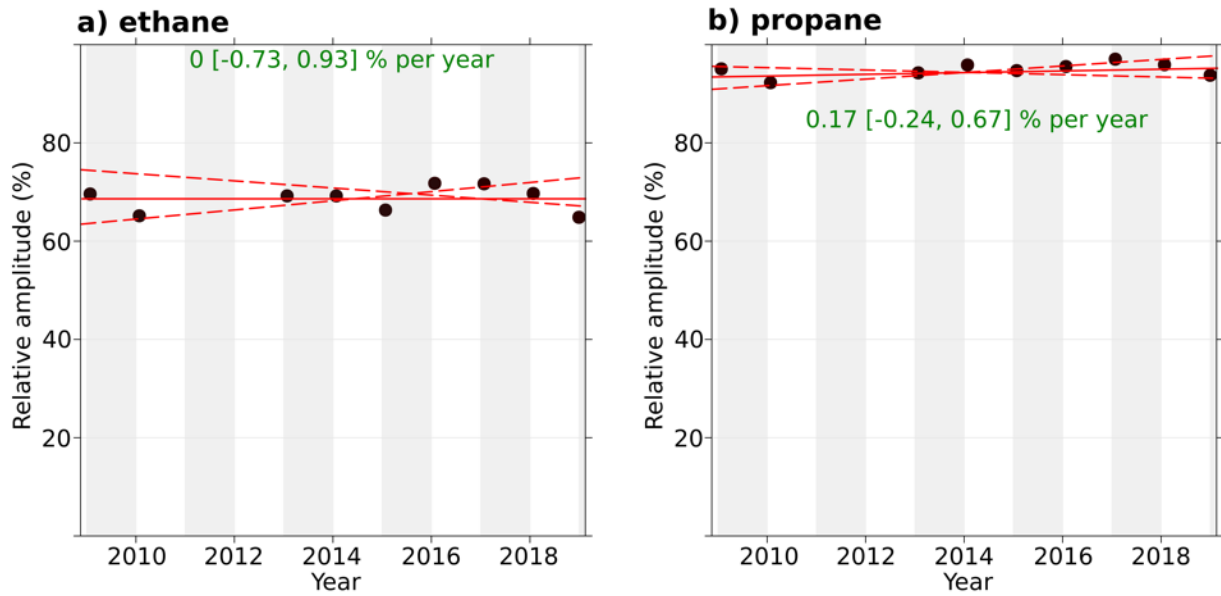


Figure 3: Trend in peak-to-peak seasonal amplitude of **a)** ethane and **b)** propane at GEOSummit, calculated as the relative difference between the maximum and minimum values from the smooth curve for each annual cycle. The solid red line shows the trend estimate and the dashed red lines show the 95 % confidence interval for the trend based on resampling methods. The overall trend is shown at the top along with the 95 % confidence interval in the slope.

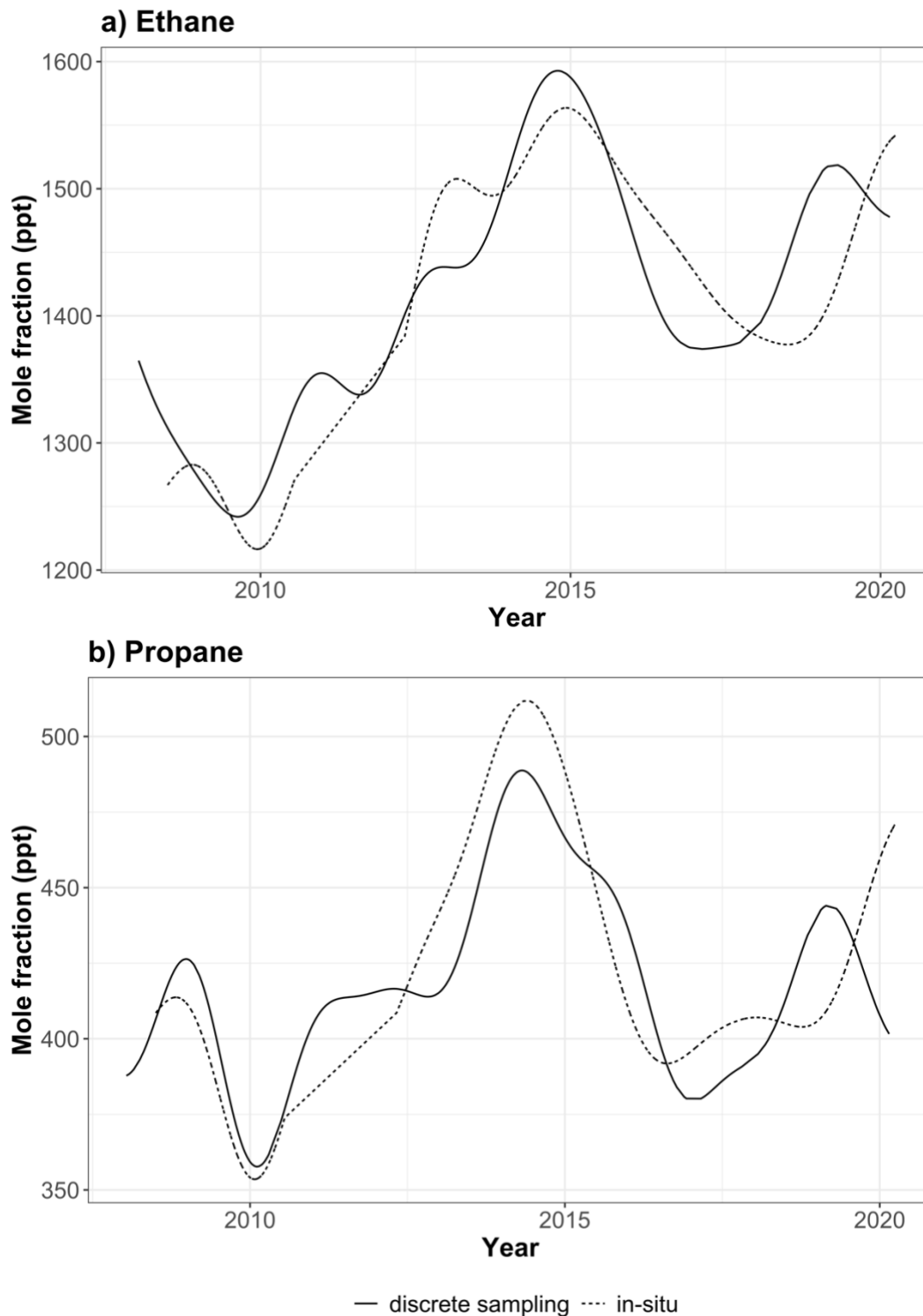


Figure 4: a) Ethane, and b) propane trends at GEOSummit from July 2008 to March 2020. Trends inferred from in-situ and discrete flask sampling are shown by the dotted and solid lines, respectively.

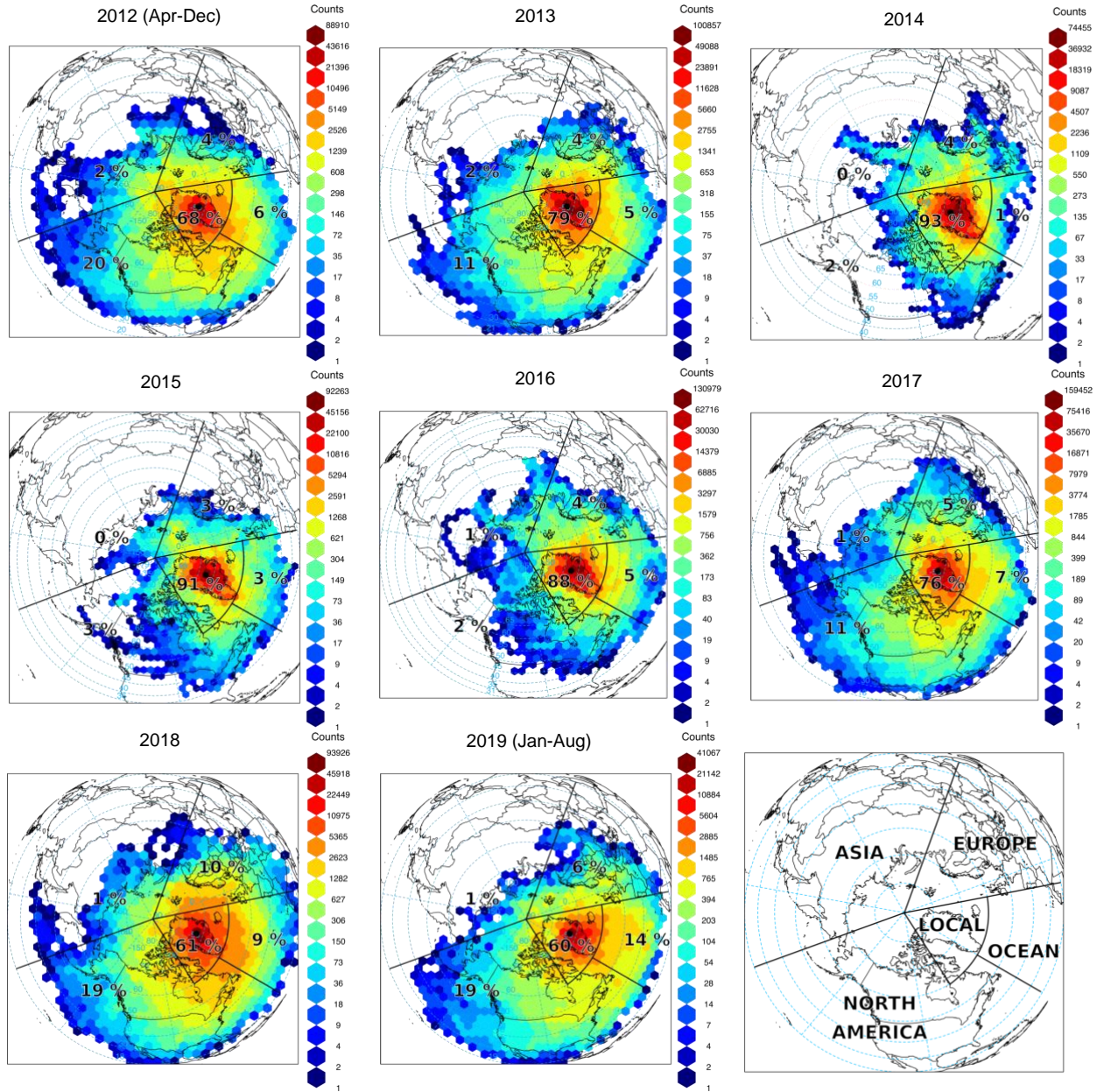


Figure 5: Origin air masses influencing GEOSummit (black dot). Gridded back trajectory frequencies using an orthogonal map projection (centered over the North Pole) with hexagonal binning. The tiles represent the number of incidences and the numbers the relative influence of the various sectors.

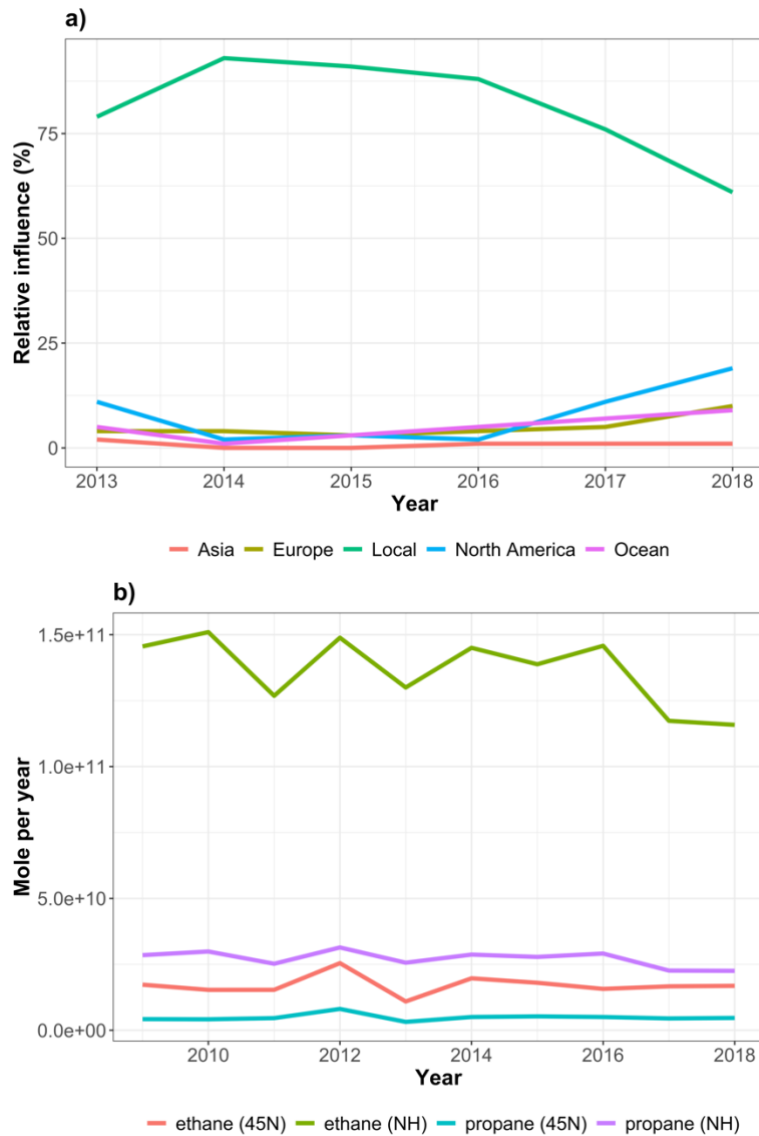


Figure 6: **a)** Annual relative contribution of different geographical sectors to air masses influencing GEOSummit according to the HYSPLIT back-trajectories analysis. **b)** Annual biomass burning emissions (in mole/year) from all open burning north of 45°N and north of the equator (Northern Hemisphere, NH) according to the Fire INventory from NCAR (FINNv2.2) emission estimates (MODIS only).

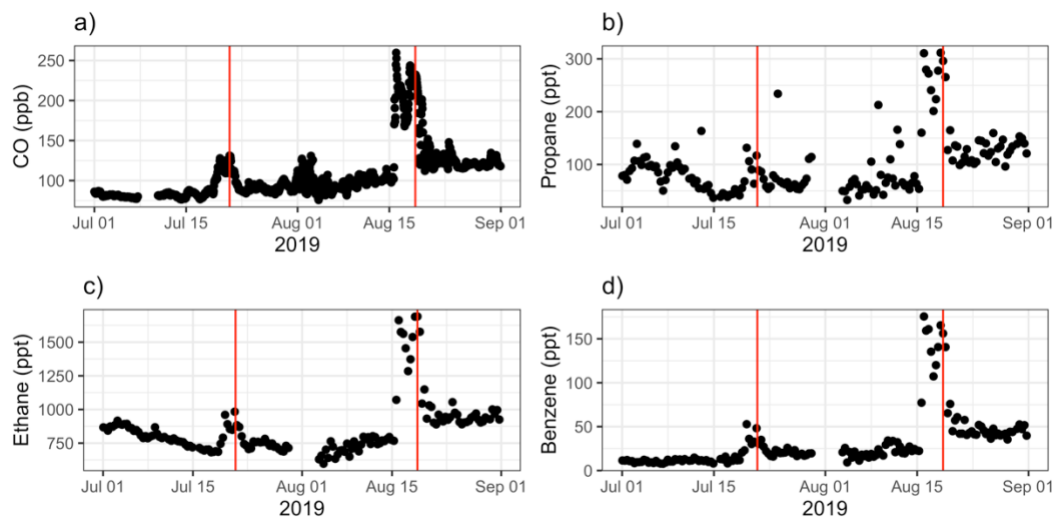


Figure 7: Time-series of **a)** carbon monoxide (CO), **b)** propane, **c)** ethane, and **d)** benzene mixing ratios in ambient air at GEOSummit in July-August 2019. The two vertical red lines show the simultaneous enhancement of mixing ratios in two biomass burning plumes.



Figure 8: U.S. field production of propane in thousand barrels per month. Data courtesy of the U.S. Energy Information Administration. The production plateaued from June 2014 to December 2016.